



This is a repository copy of *Treatment response of ethyl pyruvate in a mouse model of chronic obstructive pulmonary disease studied by hyperpolarized¹²⁹Xe MRI*.

White Rose Research Online URL for this paper:
<http://eprints.whiterose.ac.uk/160340/>

Version: Accepted Version

Article:

Kimura, A., Yamauchi, Y., Hodono, S. et al. (5 more authors) (2017) Treatment response of ethyl pyruvate in a mouse model of chronic obstructive pulmonary disease studied by hyperpolarized¹²⁹Xe MRI. *Magnetic Resonance in Medicine*, 78 (2). pp. 721-729. ISSN 0740-3194

<https://doi.org/10.1002/mrm.26458>

This is the peer reviewed version of the following article: Kimura, A., Yamauchi, Y., Hodono, S., Stewart, N.J., Hosokawa, O., Hagiwara, Y., Imai, H. and Fujiwara, H. (2017), Treatment response of ethyl pyruvate in a mouse model of chronic obstructive pulmonary disease studied by hyperpolarized ¹²⁹Xe MRI. *Magn. Reson. Med.*, 78: 721-729, which has been published in final form at <https://doi.org/10.1002/mrm.26458>. This article may be used for non-commercial purposes in accordance with Wiley Terms and Conditions for Use of Self-Archived Versions.

Reuse

Items deposited in White Rose Research Online are protected by copyright, with all rights reserved unless indicated otherwise. They may be downloaded and/or printed for private study, or other acts as permitted by national copyright laws. The publisher or other rights holders may allow further reproduction and re-use of the full text version. This is indicated by the licence information on the White Rose Research Online record for the item.

Takedown

If you consider content in White Rose Research Online to be in breach of UK law, please notify us by emailing eprints@whiterose.ac.uk including the URL of the record and the reason for the withdrawal request.



eprints@whiterose.ac.uk
<https://eprints.whiterose.ac.uk/>



Treatment response of ethyl pyruvate in a mouse model of chronic obstructive pulmonary disease studied by hyperpolarized ¹²⁹Xe MRI

Journal:	<i>Magnetic Resonance in Medicine</i>
Manuscript ID	MRM-16-16948.R1
Wiley - Manuscript type:	Full Paper
Date Submitted by the Author:	n/a
Complete List of Authors:	Kimura, Atsuomi Yamauchi, Yukiko Hodono, Shota Stewart, Neil; University of Sheffield, Unit of Academic Radiology Hosokawa, Osamu Hagiwara, Yu Imai, Hirohiko Fujiwara, Hideaki
Research Type:	Hyperpolarized imaging < Technique Development < Technical Research, Translational Research < Physiological Research
Research Focus:	Pathology < Function < Other tissues (body fluids, skin, vessels, arteries, other organs, etc)

SCHOLARONE™
Manuscripts

1
2
3 **Treatment response of ethyl pyruvate in a mouse model of chronic obstructive**
4 **pulmonary disease studied by hyperpolarized ^{129}Xe MRI**
5
6

7
8 Atsuomi Kimura,*¹ Yukiko Yamauchi,¹ Shota Hodono,¹ Neil James Stewart,² Osamu
9
10 Hosokawa,¹ Yu Hagiwara,¹ Hirohiko Imai,³ and Hideaki Fujiwara¹
11

12
13
14 ¹ Department of Medical Physics and Engineering, Division of Medical Technology
15 and Science, Faculty of Health Science, Graduate School of Medicine, Osaka
16
17 University
18

19
20
21 ² Academic Unit of Radiology, University of Sheffield, Sheffield, South Yorkshire, UK
22

23
24 ³ Research and Educational Unit of Leaders for Integrated Medical System, Center for
25 the Promotion of Interdisciplinary Education and Research, Kyoto University, Kyoto,
26
27 Japan
28
29

30
31
32 Running head:

33
34 HPXe MRI of murine COPD model and therapy response
35
36

37
38
39 Word count: 4492
40
41

42
43
44 *Corresponding author: Atsuomi Kimura, PhD, Department of Medical Physics and
45 Engineering, Division of Medical Technology and Science, Faculty of Health Science,
46 Graduate School of Medicine, Osaka University, 1-7 Yamadaoka, Suita, Osaka
47
48 565-0871, Japan,
49

50
51 Phone: +81-6-6879-2478, E-mail: kimura@sahs.med.osaka-u.ac.jp
52

ABSTRACT

Purpose: To investigate disease progression and treatment response in a murine model of chronic obstructive pulmonary disease (COPD) using a preclinical hyperpolarized ^{129}Xe (HPXe) MRI strategy.

Methods: COPD phenotypes were induced in 32 mice by 10 weeks of exposure to cigarette smoke (CS) and lipopolysaccharide (LPS). The efficacy of ethyl pyruvate (EP), an anti-inflammatory drug, was investigated by administering EP to 16 of the 32 mice after 6 weeks of CS and LPS exposure. HPXe MRI was performed to monitor changes in pulmonary function during disease progression and pharmacological therapy.

Results: HPXe metrics of fractional ventilation and gas-exchange function were significantly reduced after 6 weeks of CS and LPS exposure compared to sham-instilled mice administered with saline ($P < 0.05$). After this observation, EP administration was started in 16 of the 32 mice and continued for 4 weeks. EP was found to improve HPXe MRI metrics to a similar level as in sham-instilled mice ($P < 0.01$). Histological analysis showed significant alveolar tissue destruction in the COPD group, but relatively normal alveolar structure in the EP and sham-instilled groups.

Conclusion: This study demonstrates the potential efficacy of EP for COPD therapy, as assessed by a non-invasive, translatable ^{129}Xe MRI procedure.

Abstract word count: 200

Keywords: Hyperpolarized ^{129}Xe MRI, lung functional assessment, murine chronic obstructive pulmonary disease, treatment response, ethyl pyruvate

INTRODUCTION

Chronic obstructive pulmonary disease (COPD), a heterogeneous lung disease characterized by both chronic airway inflammation and emphysematous alveolar tissue destruction, is predicted to be the third leading cause of death worldwide by 2020 (1). At present, pharmacological therapies for COPD have shown limited efficacy and thus the development of new therapeutic drugs is vital for improving patient outcomes (2). The use of appropriate animal models of COPD that adequately induce the key symptoms of the disease is indispensable for therapy development, and rodent models are especially important. In particular, preclinical studies with mice are often appropriate because a wide range of well-characterized disease models is available (3,4). As smoking and repeated lung infections are the primary causes of COPD, several murine COPD models have been developed by exposing mice to cigarette smoke. Despite certain models showing good reproducibility for inducing the two main phenotypes of COPD mentioned above, the lack of applicable methods for assessment and diagnosis of these disease models remains a limiting factor for preclinical studies. Most previous studies have relied on plethysmography and/or histology to evaluate the applicability of murine COPD models, necessitating a tracheostomy and/or mouse death for each examination (5,6) and hence making it difficult to evaluate drug efficacy repetitively and longitudinally. To help resolve this problem, non-invasive imaging techniques that allow the longitudinal assessment of disease progression and therapeutic efficacy of drugs in vivo are required.

MRI using hyperpolarized (HP) noble gases (^3He and ^{129}Xe) as contrast agents offers an attractive means to visualize and quantitatively evaluate pulmonary functional parameters such as ventilation and gas-exchange (7-9). In a number of studies in small animals and humans, pathological changes of these fundamental

1
2
3 parameters have been investigated using HP gas MRI and quantitative measures of
4 ventilation and gas-exchange dysfunction caused by COPD have been established
5 (10,11). HP ^{129}Xe (HPXe) is a versatile contrast agent to evaluate drug efficacy in the
6 lungs because it allows not only imaging of ventilation, but also the assessment of
7 pulmonary gas-exchange, thanks to its solubility in pulmonary tissues and blood. To
8 this end, we have developed a continuous-flow mode polarizer for HPXe production
9 and have established non-invasive MRI procedures under spontaneous respiration for
10 the assessment of pulmonary function in mice (12,13). In this study, we apply our
11 HPXe methodology to explore the feasibility of a new drug for COPD therapy.
12
13
14
15
16
17
18
19
20
21
22
23

24 Ethyl pyruvate (EP), an anti-inflammatory agent, is a candidate for
25 pharmacological therapy of COPD. In recent years, EP has been shown to demonstrate
26 therapeutic efficacy in various animal models of lung diseases, such as acute lung
27 injury (ALI) and pulmonary arterial hypertension (PAH) (15-17). The therapeutic
28 efficacy of EP is attributed to its ability to regulate high-mobility group box protein-1
29 (HMGB1) release from innate immune cells, and to deactivate subsequent cytokine
30 production that would further stimulate inflammatory responses (18,19). HMGB1,
31 which is an abundant chromatin protein, may play a crucial role in pharmacological
32 therapy of COPD because it is known to not only trigger inflammatory responses but
33 also, paradoxically, to activate cells involved in tissue repair (20-24). HMGB1
34 functions by binding with the receptor for advanced glycation end products (RAGE)
35 and Toll-Like Receptors 2 and 4. In recent years, it has been shown that HMGB1 can
36 also initiate wound healing processes through binding with RAGE followed by
37 activation of the extracellular signal-regulated kinase 1/2 (ERK1/2) signaling pathway
38 (23). RAGE is expressed in pulmonary tissues with relatively high basal levels (22),
39 and EP has been reported to activate the ERK1/2 signaling pathway (14). Thus, EP
40
41
42
43
44
45
46
47
48
49
50
51
52
53
54
55
56
57
58
59
60

1
2
3 shows considerable potential as a drug for lung tissue repair accompanied with
4 anti-inflammatory responses through regulation of the HMGB1/RAGE pathway.
5
6

7
8 In the present study, we demonstrate the observation of disease progression in a
9 mouse model of COPD induced by cigarette smoke (CS) exposure and
10 lipopolysaccharide (LPS) instillation, as measured by HPXe MRI. Additionally, the
11 efficacy of ethyl pyruvate (EP) for treatment of this COPD model is studied to assess
12 the feasibility of this non-invasive imaging technique as a diagnostic method for early
13 disease detection and therapy response evaluation in COPD.
14
15
16
17
18
19
20
21
22

23 **METHODS**

24 **Animal preparation**

25
26 Thirty-seven male, 6-week-old, type ddY mice, weighing 30 – 35 g (Japan SLC, Inc.,
27 Shizuoka, Japan) were included in this study. All experimental procedures and animal
28 care standards conformed to Osaka University guidelines. Mice were divided into two
29 groups: a sham-instilled group of N=5 mice and a CS and LPS group of N=32. The CS
30 and LPS mice were further divided into 2 equal groups of 16 individuals. The two
31 subgroups were separately administered with a combination of CS and LPS as follows.
32 CS of approximately 2.1 L in volume resulting from one cigarette (Lark Milds: tar 9
33 mg, nicotine 0.8 mg; Philip Morris International Inc., New York, USA) was collected
34 into a Tedlar® bag (Sigma-Aldrich, St Louis, MO, USA). The mice in each subgroup
35 were placed in a semi-sealed plastic container with a volume of 12.4 L and 9 airshafts
36 of 5 mm inner diameter on its upper surface. CS was flowed from the Tedlar® bag into
37 the container for 26 minutes at a rate of 40 mL/min. Following this, fresh room air was
38 flowed into the container for 5 minutes (at 720 mL/min). This whole-body exposure
39
40
41
42
43
44
45
46
47
48
49
50
51
52
53
54
55
56
57
58
59
60

1
2
3
4 procedure was performed twice daily on five consecutive days within one week, and
5
6 repeated on a weekly basis as described below. On each fifth day, a 20 μ L solution of
7
8 LPS in saline (0.4 mg/kg, LPS in *Escherichia coli*, serotype O55:B5, Sigma-Aldrich,
9
10 St. Louis, MO, USA) was delivered intra-tracheally to the mice at least 2 hours prior
11
12 to the CS exposure. The sham-instilled mice were intra-tracheally administered with
13
14 20 μ L of saline on every fifth day in the same manner as the LPS administration.
15
16

17
18 Six weeks after commencing CS and LPS exposure, the two subgroups of CS and
19
20 LPS mice were assigned as follows: a pure CS and LPS group of N=16 mice and an
21
22 EP-treated group of N=16 mice. For the pure CS and LPS group, the same protocol of
23
24 CS and LPS administration was continued for a further 4 weeks. EP-treated mice were
25
26 intra-tracheally administered with a 20 μ L solution of EP in saline (1.3 mg/kg, Tokyo
27
28 Chemical Industry Ltd, Tokyo, Japan) on a daily basis for 4 weeks, in addition to the
29
30 continued administration of CS and LPS as detailed above. EP was always
31
32 administered after the CS and LPS exposure, separated by an interval of at least 2
33
34 hours. Therefore, in total, 10 weeks were required to completely prepare the CS and
35
36 LPS, and EP-treated groups. The sham-instilled mice were intra-tracheally
37
38 administered with 20 μ L of saline per day, every weekday, for this 4 week period, in
39
40 the same manner as the EP treatment. The survival rates of the whole 10-week
41
42 procedure were 75% for CS and LPS mice (12 out of 16 mice survived), 75% for
43
44 EP-treated mice (12 out of 16 mice survived), and 100 % for the sham-instilled group.
45
46
47
48

49
50 In all cases, prior to the instillation of saline, LPS or EP solution, mice were
51
52 anesthetized with 2% isoflurane (ISOFLU®, Dainippon Sumitomo Pharmaceutical Co.
53
54 Ltd, Osaka, Japan), which was administered via a nose cone using a home-built
55
56 anesthesia system connected to an isoflurane vaporizer (Isorex I-200, Shin-Ei
57
58
59
60

1
2
3 Industries, Inc., Tokyo, Japan). Subsequently, mice were intubated with a 22 G
4 catheter (SURFLO® F&F, Terumo Corp., Tokyo, Japan) while positioned supine and
5 secured to a slanted wooden board, and then the saline, LPS or EP solution was
6 instilled.
7
8
9
10

11
12 MR measurements of sham-instilled and CS and LPS groups were performed at 0
13 weeks (prior to the first administration) and 2, 6, 8 and 10 weeks after commencing the
14 administration of CS and LPS. Similarly, MR measurements of the EP-treated group
15 were performed at 0, 6, 8 and 10 weeks after commencing the administration of CS and
16 LPS (i.e. -6, 0, 2 and 4 weeks from commencement of EP therapy). Immediately before
17 all MR measurements, mice were anesthetized with 2% isoflurane as detailed above. A
18 plastic mouth mask, to which three polyethylene tubes were connected (for HPXe gas
19 delivery, O₂ delivery and exhaled gas exhaust), was attached to the animal prior to
20 placement in the MR scanner. In order to synchronize image acquisitions with
21 respiratory motion, a pulse transducer (AD Instruments Ltd., Dunedin, New Zealand)
22 was positioned on the mouse abdomen, just inferior to the diaphragm. This sensor
23 converted the respiratory motion into an electrical signal that was monitored in
24 real-time using LabVIEW software (National Instruments, Austin, TX, USA). The
25 animal's body temperature in the magnet was maintained with warm water circulating
26 through a rubber tube placed on the abdomen. The MR imaging procedure was
27 performed without tracheal intubation or tracheotomy and hence was entirely
28 non-invasive.
29
30
31
32
33
34
35
36
37
38
39
40
41
42
43
44
45
46
47
48
49
50
51
52

53 ¹²⁹Xe Polarization and Gas Delivery

54
55
56
57
58
59
60

¹²⁹Xe nuclei were polarized to ~10% by Rb-¹²⁹Xe spin-exchange optical pumping (25) with a home-built continuous-flow ¹²⁹Xe polarizer (26). A gas mixture consisting of 70% Xe (natural abundance, comprising 26% ¹²⁹Xe) and 30% N₂ was supplied from a pre-mixed cylinder (Air Liquid Japan Ltd., Tokyo, Japan) at a pressure of 0.15 atmospheres for ¹²⁹Xe polarization. Once polarized, HPXe was subsequently compressed to atmospheric pressure with a diaphragm pump (LABOPORT® N86 KN.18, KNF Neuberger GmbH, Freiburg, Germany) to facilitate gas delivery directly and continuously from the polarizing cell to the mouse in the magnet. The HPXe gas mixture was flowed continuously at a rate of 50 mL/min to each mouse and was mixed with O₂ (continuously supplied at 9 mL/min) in the mouth mask. The percentages of Xe and O₂ spontaneously inhaled by the mice were 59.3% and 15.3%, respectively.

MR Imaging

All MR measurements were performed on a Agilent Unity INOVA 400 WB high-resolution NMR spectrometer system running VNMR 6.1C software (Varian Inc., Palo Alto, CA, USA). A 9.4 T vertical magnet with a bore width of 89 mm (Oxford Instruments Plc., Oxford, UK) was used. A self-shielded gradient probe was employed in combination with Litz volume RF coils of 34 mm inner diameter, tunable to the Larmor frequencies of ¹²⁹Xe (110.6 MHz) and ¹H (399.6 MHz) (Clear Bore DSI-1117, Doty Scientific, Inc., Columbia, SC, USA).

For assessment of pulmonary ventilation and gas-exchange function, HPXe gas images were acquired with a 2D multi-shot balanced steady-state free precession (bSSFP) sequence, which was programmed in-house (27). Acquisition parameters were as follows: RF pulse, 1000 μs long Gaussian-shaped pulse with a bandwidth of 2800 Hz and centered on the ¹²⁹Xe gas-phase resonance (0 ppm); TR/TE, 3.2/1.6 ms;

1
2
3 receiver bandwidth, 62 kHz; one coronal slice of thickness 20 mm, covering the whole
4 of the lungs; matrix size, 64×32 ; field of view, $80 \times 25.6 \text{ mm}^2$; number of shots
5 (required to fill k-space), 4; flip angle, 40° ; number of averages of the whole
6 acquisition, 8; centrically-ordered phase encoding. ^{129}Xe images were reconstructed
7 by a 2D fast Fourier transform after zero filling to a 128×64 matrix using in-house
8 MATLAB scripts (MathWorks Inc., Natick, MA, USA).
9
10
11
12
13
14
15

16 17 18 19 **Evaluation of ventilation function**

20 For evaluating pulmonary ventilation function, the fractional ventilation (i.e. the
21 fraction of gas “turned over” per breathing cycle), r_a , was mapped across the lungs
22 following a previously reported method (28,29). Briefly, after the HPXe concentration
23 in the lungs had reached a steady-state under the continuous supply of HPXe and O_2 ,
24 two pre-saturation RF pulses were applied at the ^{129}Xe gas-phase frequency to destroy
25 any gas-phase ^{129}Xe magnetization in the alveoli. The bSSFP imaging sequence was
26 then used to acquire respiratory-synchronized ^{129}Xe gas ventilation images at
27 inspiration after n breathing cycles. The value of n was sequentially incremented from
28 1 to 10, and then to 12, 15 and 20; thus, thirteen ^{129}Xe ventilation images were
29 acquired in total. (In Reference (28), images were acquired after 1 to 10 breaths only;
30 the purpose of the additional acquired images here was to improve the accuracy of the
31 r_a estimate.) From the resulting image series, the fractional ventilation of each voxel
32 was evaluated by analyzing the dependency of the ^{129}Xe MR signal intensity upon the
33 number of breaths (Equations 2 and 3, Reference (28)). The fractional ventilation, r_a ,
34 is defined as:
35
36
37
38
39
40
41
42
43
44
45
46
47
48
49
50
51
52
53
54

$$55 \quad r_a = \frac{V_f}{V_o + V_f}, \quad [1]$$

where V_o and V_f denote the volumes of old and new (fresh) gas within the voxel after each breath, respectively. r_a values were determined pixel-by-pixel over the whole image to derive a r_a map, and averaged for each mouse to obtain the whole lung r_a . Finally, the whole lung r_a values were averaged for each of the sham-instilled, CS and LPS, and EP-treated groups to obtain group mean r_a values.

Evaluation of gas-exchange function

The efficiency of HPXe gas-exchange between the alveoli (gas-phase) and the lung parenchyma and capillaries (dissolved-phase) was evaluated by the xenon polarization transfer contrast (XTC) method (30). Briefly, a XTC image was generated by acquiring bSSFP gas ventilation images at expiration, separated by the application of four frequency-selective inversion pulses (inter-pulse delay 20 ms) at the Larmor frequency of dissolved-phase ^{129}Xe (197 ppm), and comparing the resulting ventilation image intensities (27). The flip angle of the inversion pulse (Gaussian-shape; 1000 μs duration) was calibrated prior to the present study. Similarly, a “control” bSSFP image was generated by acquiring ventilation images at expiration, separated by the application of the same inversion pulses, but centered at -197 ppm instead of 197 ppm. The whole XTC measurement was repeated three times, and the three images were summed to improve image SNR. The parameter of gas-exchange function, f_D , defined as the fractional depolarization of gas-phase HPXe caused by the repeated RF inversion of dissolved-phase HPXe during continuous diffusive exchange of xenon between the two compartments, was calculated according to the ratio of the signal intensities of control and XTC images as follows:

$$f_D(\%) = \left(1 - \sqrt[N]{\frac{S_{XTC}}{S_{control}}}\right) \times 100 \quad [2]$$

where S_{XTC} and $S_{control}$ are the signal intensities of XTC and control images,

1
2
3 respectively, and N is the number of inversion pulses. f_D values were calculated on a
4 pixel-by-pixel basis in order to create a whole lung f_D map. As with the r_a analysis,
5 mean f_D values were obtained for each of the sham-instilled, CS and LPS, and
6 EP-treated groups.
7
8
9
10
11

12
13
14 For each of the above described techniques, the existence of statistically-significant
15 differences in mean values of derived parameters between groups was assessed by the
16 analysis of variance (ANOVA) method with the Tukey-Kramer test, using the JMP
17 Statistics package (SAS Institute Inc., Cary, NC, USA).
18
19
20
21
22
23

24 25 26 **Histological Analysis**

27
28 After completion of the MR experiments (week 10), the mice were euthanized with a
29 lethal dose of carbon dioxide gas. Lungs were extracted and fixed in a 10 % formalin
30 solution, and hematoxylin and eosin (H&E) stained slides were created to analyze
31 morphological changes to the alveoli and terminal bronchioles. Four slides per mouse
32 were used to evaluate structural parameters including mean linear intercept (MLI) and
33 mean bronchial wall thickness (h), as previously described (31). Five MLI and h
34 values were calculated from each slide, corresponding to the five lobar regions of the
35 lung (right upper lobe, right middle lobe and right lower lobe; left upper lobe and left
36 lower lobe). Each set of five values was averaged over the four slides, and then the
37 resulting five averaged regional MLI and h values were in turn averaged to yield a
38 single MLI and h value for each mouse. Mean MLI and h values were calculated for
39 each of the sham-instilled, CS and LPS, and EP-treated groups in this manner.
40
41
42
43
44
45
46
47
48
49
50
51
52
53
54

55 In order to monitor morphological changes during the 10 weeks of CS and LPS
56 administration, one additional CS and LPS histological analysis group (N=3 mice) was
57
58
59

1
2
3 prepared after 4 weeks of administration using the same protocol as described above.
4
5 MLI and h values were evaluated for these groups as described above.
6
7
8
9

10 RESULTS

11
12 Figures 1 and 2 show the longitudinal changes in r_a and f_D maps, respectively, after 0,
13
14 6, 8 and 10 weeks of CS and LPS administration, for one representative mouse from
15
16 each of the sham-instilled, CS and LPS, and EP-treated groups. It should be noted that
17
18 Figures 1 and 2 were additionally processed with a 2 x 2 median filter using ImageJ
19
20 (National Institute of Health) to reduce the prevalence of artifacts associated with
21
22 cardiac motion and rapid diffusion of HPXe in the major airways. These maps depict
23
24 the regional variation in pulmonary ventilation and gas-exchange functional changes
25
26 over time. In particular, they highlight an approximately spatially homogeneous
27
28 reduction of r_a in the CS and LPS mice after 10 weeks, and an overall improvement in
29
30 r_a and f_D in response to EP therapy, with some regional heterogeneity.
31
32
33
34

35
36 Figures 3 and 4 display the group-mean values of r_a and f_D , respectively, after 0,
37
38 2, 6, 8 and 10 weeks of CS and LPS exposure. The mean r_a value for the CS and LPS
39
40 group was found to be significantly decreased compared to that of the sham-instilled
41
42 group after 6 weeks ($P < 0.05$), and was observed to continue to decrease for the
43
44 remainder of the 10 week measurement period (after 10 weeks, $r_{a,CS\&LPS} = 0.19 \pm 0.03$,
45
46 compared with $r_{a,Sham-instilled} = 0.25 \pm 0.03$, $P < 0.01$). The mean r_a value of the EP
47
48 group was comparable to that of the sham-instilled mice ($r_{a,EP} = 0.25 \pm 0.03$) after 10
49
50 weeks, i.e. 4 weeks of EP administration. This value is also significantly larger than
51
52 that of the CS and LPS group; $P < 0.01$. The f_D value of the CS and LPS group
53
54 ($f_{D,CS\&LPS} = 4.5 \pm 1.1$ %) was significantly lower ($P < 0.01$) than that of the
55
56 sham-instilled group ($f_{D,Sham-instilled} = 6.8 \pm 0.6$ %) after 10 weeks of exposure to CS
57
58
59
60

1
2
3 and LPS, while the f_D value of the EP group was considerably improved ($f_{D,EP} = 6.2 \pm$
4 0.9 %) compared with that of the CS and LPS group ($P < 0.01$). The longitudinal
5
6 variation in mean r_a and f_D values from all groups was found to correlate significantly
7
8 (Pearson's $r = 0.820$, $P < 0.01$).
9

10
11
12 Figures 5 and 6 depict whole lung mean MLI and h values and representative
13
14 histological images obtained from mice from each of the sham-instilled, EP-treated
15
16 and CS and LPS groups at the end of the 10 week experimental protocol, and the
17
18 histological analysis group, respectively. As illustrated in these figures, an
19
20 enlargement of the alveolar airspace volume was observed at week 10 following
21
22 bronchial wall thickening; this is discussed below. The mean MLI of the CS and LPS
23
24 group ($MLI_{CS\&LPS} = 44.0 \pm 3.8 \mu\text{m}$) was significantly larger than that of the
25
26 sham-instilled group ($MLI_{Sham-instilled} = 39.7 \pm 1.8 \mu\text{m}$, $P < 0.05$). The mean MLI of the
27
28 EP-treated group ($MLI_{EP} = 38.2 \pm 2.4 \mu\text{m}$) was smaller than that of the CS and LPS
29
30 group ($P < 0.01$) and similar to that of the sham-instilled group. The h value of the
31
32 EP-treated group ($h_{EP} = 12.5 \pm 1.1 \mu\text{m}$) was smaller than that of the CS and LPS group
33
34 ($h_{CS\&LPS} = 14.9 \pm 1.3 \mu\text{m}$, $P < 0.01$), and similar to that of the sham-instilled group
35
36 ($h_{Sham-instilled} = 12.3 \pm 0.6 \mu\text{m}$) at week 10. Meanwhile, the mean MLI and h values of
37
38 the histological analysis group (exposed to CS and LPS for 4 weeks) were $MLI_{HA_4w} =$
39
40 $39.8 \pm 2.5 \mu\text{m}$ and $h_{HA_4w} = 14.1 \pm 0.6 \mu\text{m}$, respectively, which were comparable to
41
42 those of the sham-instilled mice.
43
44
45
46
47

48
49 Figure 7 shows correlation plots of individual r_a , f_D , h and MLI values obtained
50
51 from the sham-instilled, EP-treated and CS and LPS mice after the 10 week
52
53 experimental protocol. Significant positive correlations were observed between r_a and
54
55 f_D , and MLI and h , as were significant negative correlations between r_a and h , f_D and h ,
56
57 and f_D and MLI ($P < 0.05$). The correlation between r_a and MLI was not statistically
58
59

1
2
3 significant ($P > 0.05$).
4
5
6

7 8 **DISCUSSION**

9
10 In the present study, a murine model of COPD was developed by 10 weeks of exposure
11 to CS and LPS, and the associated induced temporal changes of pulmonary ventilation
12 and gas-exchange function were assessed noninvasively by HPXe MRI. The present
13 COPD model was able to induce characteristic emphysematous alveolar tissue
14 destruction, achieved by modifying previous protocols for producing airway
15 inflammation using CS and LPS (21,32,33). The longitudinal HPXe MRI assessment of
16 pulmonary function revealed a significant decrease in parameters of both fractional
17 ventilation, r_a , and gas-exchange, f_D , of the CS and LPS mice after 6 weeks of CS and
18 LPS exposure. However, for the first 2 weeks, pulmonary function in these mice was
19 not notably different from that of sham-instilled mice. The longitudinal variation in
20 the mean values of the two parameters was found to correlate, suggesting that the
21 time-course of disease progression acted to simultaneously impair both ventilation and
22 gas-exchange function. In addition, the r_a and f_D values were found to correlate
23 significantly on a per mouse basis at week 10, although not prior to week 10, which
24 supports the decision to end the CS and LPS administration at this time-point.
25 Reductions in f_D and increases in the prevalence of ventilation defects have been
26 previously observed using hyperpolarized gas MRI in human COPD patients (34,35),
27 supporting the fact that the CS and LPS model of COPD employed here could
28 successfully induce similar pathological effects to COPD itself. Combining
29 whole-body CS exposure with LPS administration induced significant emphysematous
30 pathology and bronchial wall thickening after 10 weeks of exposure, as illustrated by
31 histology slides (Figures 5 and 6). On the other hand, exposure to only CS has been
32
33
34
35
36
37
38
39
40
41
42
43
44
45
46
47
48
49
50
51
52
53
54
55
56
57
58
59
60

1
2
3 reported to typically require ≥ 6 months to establish the characteristic emphysematous
4 pathology in mice (36). While Hansbro et al. succeeded to establish a mouse model of
5 COPD by 8 weeks of CS exposure through the nose only, this procedure required
6 purpose-built equipment that is not readily translatable to our laboratory, and the CS
7 dose was relatively high (2 cigarettes/mouse/day) (37). Thus, our protocol of CS and
8 LPS exposure considerably shortened the time required to produce the two phenotypes
9 of COPD pathology without necessitating specialist equipment. As such, this
10 procedure may be advantageous for future investigations of COPD treatment response.
11
12
13
14
15
16
17
18
19
20

21 The present COPD mouse model caused significant decreases of ventilation and
22 gas-exchange parameters: mean r_a of 0.19 ± 0.03 in CS and LPS mice compared with
23 0.25 ± 0.03 in sham-instilled mice; mean f_D of $4.5 \pm 1.0\%$ compared with $6.8 \pm 0.6\%$,
24 respectively, after 10 weeks. The decrease of r_a after 10 weeks of exposure to CS and
25 LPS is indicative of an increase in the bronchial wall thickness, and indeed r_a showed
26 a significant correlation with the histology-derived h value at this time-point (Figure
27 7). However, the decrease of f_D is indicative of both a reduction in the volume of
28 septal tissue and an increase in the bronchial wall thickness. The decrease in f_D and r_a
29 at the 6 week time-point may be attributable to the increase in bronchial wall thickness,
30 h , (see Supporting Figure S1) since it is unlikely that the volume of septal tissue
31 decreased (as there was no significant change in MLI at the 4 week time-point). This
32 situation may be similar to a previous study in which CS and LPS were administered to
33 rats for 6 weeks (21). According to that report, no histological evidence of COPD (i.e.
34 MLI change) was seen despite overexpression of HMGB1. However, it is worth noting
35 that these observations might not exclude the possibility of early stage emphysema,
36 because mice lack the anatomical characteristics (respiratory bronchioles) for
37 expression of centrilobular emphysema (4). One might also expect that the decrease in
38
39
40
41
42
43
44
45
46
47
48
49
50
51
52
53
54
55
56
57
58
59
60

1
2
3
4 f_D was caused in part by a reduction in the volume of the pulmonary capillaries,
5
6 because the f_D measurement includes a contribution related to blood volume (since
7
8 ddY-type mice exhibit only a single NMR peak from dissolved-phase ^{129}Xe in lung
9
10 tissue and blood (31), and furthermore, the XTC technique as employed herein does
11
12 not enable the distinction of two dissolved-phase ^{129}Xe compartments even if they
13
14 were present).
15
16

17
18 In the present study, the efficacy of EP for treatment of the CS and LPS model of
19
20 COPD was quantified by longitudinal observations of pulmonary function. The
21
22 reductions in r_a and f_D in the CS and LPS group after 6 weeks recovered to a similar
23
24 level as the sham-instilled group by 2 and 4 weeks of administration of EP,
25
26 respectively ($P < 0.01$, see Figures 3 and 4). Because the administration of EP was
27
28 only started 6 weeks after commencement of CS and LPS exposure (i.e. after some
29
30 impairment of pulmonary function was observed), EP likely exhibited a combination
31
32 of both preventative and therapeutic properties in the CS and LPS model of COPD. In
33
34 other words, EP may have acted to inhibit further emphysema development and to
35
36 repair the existing bronchial wall damage (Figures 5 and 6). This hypothesis is
37
38 supported by the lack of significant difference in the r_a and f_D values between 6 and 10
39
40 week time-points in the EP-treated group ($P > 0.05$). However, the present study was
41
42 unable to clarify whether the recovery of HPXe MRI metrics might be indicative of the
43
44 reparation of tissue loss by early emphysema and/or improved pulmonary
45
46 hemodynamics. To prove whether EP can indeed act to reverse emphysematous tissue
47
48 loss, further experiments are needed in which EP administration is started after 10
49
50 weeks of CS and LPS exposure.
51
52
53
54

55
56 To the best of our knowledge, this is the first evidence of the therapeutic action
57
58 of EP in a murine COPD model, as measured by HPXe MRI. Recently, it has been
59
60

1
2
3 reported that intraperitoneal administration of EP can inhibit the expression of
4
5 HMGB1 (18,19). Additionally, high expression of HMGB1 has been reported to lead to
6
7 lung functional impairment, and is associated with the development and progression of
8
9 COPD (20-22). On the other hand, albeit paradoxically, the HMGB1/RAGE pathway is
10
11 also known to be associated with a series of signalling pathways for tissue repair
12
13 (23,24). It may be speculated that EP is effective in treating lung diseases caused by
14
15 chronic inflammation (such as the CS and LPS model of COPD) through the regulation
16
17 of HMGB1/RAGE, leading to improvement and potentially maintenance of murine
18
19 pulmonary function. Further studies with corresponding molecular assays are required
20
21 to substantiate this claim.
22
23
24

25 26 27 28 **CONCLUSION**

29
30 The feasibility of HPXe MRI for longitudinal assessment of disease progression and
31
32 pharmacological therapy has been demonstrated in a mouse model of COPD. The
33
34 model, combining exposure to cigarette smoke and lipopolysaccharide solution,
35
36 induced COPD characteristics in mice in a relatively short time of 10 weeks and offers
37
38 potential advantages for pharmacological therapy assessment applications. HPXe
39
40 MRI-derived metrics of pulmonary function showed considerable impairment in both
41
42 ventilation and gas-exchange function in CS and LPS mice compared with
43
44 sham-instilled mice, as verified by histological analysis. Longitudinal HPXe MRI
45
46 assessment of the action of an anti-inflammatory agent, ethyl pyruvate, for treatment
47
48 of this COPD model revealed preliminary evidence of its efficacy, and may help to
49
50 elucidate the exact mechanisms of its therapeutic action in the future.
51
52
53
54
55
56
57
58
59
60

1
2
3 Acknowledgements
4

5 This work was supported by the Japan Society for the Promotion of Science (JSPS)
6
7
8 KAKENHI grant numbers: JP24300163 and JP15H03006. NJS acknowledges funding
9
10 support from the Medical Research Council (MRC) and the JSPS summer programme
11
12 (2015).
13
14
15
16
17
18
19
20
21
22
23
24
25
26
27
28
29
30
31
32
33
34
35
36
37
38
39
40
41
42
43
44
45
46
47
48
49
50
51
52
53
54
55
56
57
58
59
60

For Peer Review

References

1. Lozano R, Naghavi M, Foreman K, et al. Global and regional mortality from 235 causes of death for 20 age groups in 1990 and 2010: a systematic analysis for the Global Burden of Disease Study 2010. *The Lancet* 2012;380(9859):2095-2128.
2. Holgate S, Agusti A, Strieter RM, Anderson GP, Fogel R, Bel E, Martin TR, Reiss TF. Drug development for airway diseases: looking forward. *Nat Rev Drug Discov* 2015;14:367-368.
3. Fricker M, Deane A, Hansbro PM. Animal models of chronic obstructive pulmonary disease. *Expert Opin Drug Discov* 2014;9(6):629-645.
4. Gardi C, Stringa B, Martorana PA. Animal models for anti-emphysema drug discovery. *Expert Opin Drug Discov* 2015;10(4):399-410.
5. Mizutani N, Fuchikami J, Takahashi M, Nabe T, Yoshino S, Kohno S. Pulmonary emphysema induced by cigarette smoke solution and lipopolysaccharide in guinea pigs. *Biol Pharm Bull* 2009;32:1559-1564.
6. Li JJ, Wang W, Baines KJ, Bowden NA, Hansbro PM, Gibson PG, Kumar RK, Foster PS, Yang M. IL-27/IFN- γ induce MyD88-dependent steroid-resistant airway hyperresponsiveness by inhibiting glucocorticoid signaling in macrophages. *J Immunol* 2010;185(7):4401-4409.
7. Fain SB, Korosec FR, Holmes JH, O'Halloran R, Sorkness RL, Grist TM. Functional lung imaging using hyperpolarized gas MRI. *J Magn Reson Imag* 2007;25(5):910-923.
8. Mugler JP, III, Altes TA. Hyperpolarized ^{129}Xe MRI of the human lung. *J Magn Reson Imag* 2013;37(2):313-331.
9. van Beek EJR, Wild JM, Kauczor H-U, Schreiber W, Mugler JP, de Lange EE. Functional MRI of the lung using hyperpolarized 3-helium gas. *J Magn Reson Imag*

- 2004;20(4):540-554.
10. Kirby M, Pike D, Coxson HO, McCormack DG, Parraga G. Hyperpolarized ^3He ventilation defects used to predict pulmonary exacerbations in mild to moderate chronic obstructive pulmonary disease. *Radiology* 2014;273(3):887-896.
 11. Qing K, Mugler JP 3rd, Altes TA, Jiang Y, Mata JF, Miller GW, Ruset IC, Hersman FW, Ruppert K. Assessment of lung function in asthma and COPD using hyperpolarized ^{129}Xe chemical shift saturation recovery spectroscopy and dissolved-phase MRI. *NMR Biomed* 2014;27(12):1490-1501.
 12. Imai H, Kimura A, Fujiwara H. Small animal imaging with hyperpolarized ^{129}Xe magnetic resonance. *Anal Sci* 2014;30(1):157-166.
 13. Tetsumoto S, Takeda Y, Imai H, et al. Validation of noninvasive morphological and diffusion imaging in mouse emphysema by micro-computed tomography and hyperpolarized ^{129}Xe magnetic resonance imaging. *Am J Respir Cell Mol Biol* 2013;49(4):592-600.
 14. Kung CW, Lee YM, Cheng PY, Peng YJ, Yen MH. Ethyl pyruvate reduces acute lung injury via regulation of iNOS and HO-1 expression in endotoxemic rats. *J Surg Res* 2011;167(2):e323-e331.
 15. Liu C, Fang C, Cao G, Liu K, Wang B, Wan Z, Li S, Wu S. Ethyl pyruvate ameliorates monocrotaline-induced pulmonary arterial hypertension in rats. *J Cardiovasc Pharmacol* 2014;64(1):7-15.
 16. Shang GH, Lin DJ, Xiao W, Jia CQ, Li Y, Wang AH, Dong L. Ethyl pyruvate reduces mortality in an endotoxin-induced severe acute lung injury mouse model. *Respir Res* 2009;10:91.
 17. Pulathan Z, Altun G, Hemşinli D, Menteşe A, Yuluğ E, Civelek A. Role of ethyl pyruvate in systemic inflammatory response and lung injury in an experimental

- 1
2
3 model of ruptured abdominal aortic aneurysm. *Biomed Res Int* 2014;2014:857109.
4
5
6 18. Cheng P, Dai W, Wang F, Lu J, Shen M, Chen K, Li J, Zhang Y, Wang C, Yang J,
7
8 Zhu R, Zhang H, Zheng Y, Guo C-Y, Xu L. Ethyl pyruvate inhibits proliferation
9
10 and induces apoptosis of hepatocellular carcinoma via regulation of the HMGB1-
11
12 RAGE and AKT pathways. *Biochem Biophys Res Commun* 2014;443(4):1162-1168.
13
14 19. Lee YM, Kim J, Jo K, Shin SD, Kim C-S, Sohn EJ, Kim SG, Kim JS. Ethyl
15
16 Pyruvate Inhibits Retinal Pathogenic Neovascularization by Downregulating
17
18 HMGB1 Expression. *J Diabetes Res* 2013;2013:8.
19
20
21 20. Ko H-K, Hsu W-H, Hsieh C-C, Lien T-C, Lee T-S, Kou YR. High expression of
22
23 high-mobility group box 1 in the blood and lungs is associated with the
24
25 development of chronic obstructive pulmonary disease in smokers. *Respirology*
26
27 2014;19(2):253-261.
28
29
30 21. Wang CM, Jiang M, Wang HJ. Effect of NF- κ B inhibitor on high-mobility group
31
32 protein B1 expression in a COPD rat model. *Mol Med Rep* 2013;7(2):499-502.
33
34
35 22. Zhang Y, Li S, Wang G, Han D, Xie X, Wu Y, Xu J, Lu J, Li F, Li M. Changes of
36
37 HMGB1 and sRAGE during the recovery of COPD exacerbation. *J Thorac Dis*
38
39 2014;6(6):734-741.
40
41
42 23. Lee DE, Trowbridge RM, Ayoub NT, Agrawal DK. High-mobility Group Box
43
44 Protein-1, Matrix Metalloproteinases, and Vitamin D in Keloids and Hypertrophic
45
46 Scars. *Plast Reconstr Surg Glob Open* 2015;3(6):e425.
47
48
49 24. Pandolfi F, Altamura S, Frosali S, Conti P. Key Role of DAMP in Inflammation,
50
51 Cancer, and Tissue Repair. *Clin Ther* 2016;38(5):1017-1028.
52
53
54 25. Walker TG, Happer W. Spin-exchange optical pumping of noble-gas nuclei.
55
56 *Reviews of Modern Physics* 1997;69(2):629-642.
57
58 26. Imai H, Fukutomi J, Kimura A, Fujiwara H. Effect of reduced pressure on the
59
60

- 1
2
3 polarization of ^{129}Xe in the production of hyperpolarized ^{129}Xe gas: Development
4 of a simple continuous flow mode hyperpolarizing system working at pressures as
5 low as 0.15 atm. Concepts in Magnetic Resonance Part B: Magnetic Resonance
6 Engineering 2008;33B(3):192-200.
7
8
9
10
11
12 27. Imai H, Kimura A, Hori Y, Iguchi S, Kitao T, Okubo E, Ito T, Matsuzaki T,
13 Fujiwara H. Hyperpolarized ^{129}Xe lung MRI in spontaneously breathing mice with
14 respiratory gated fast imaging and its application to pulmonary functional imaging.
15 NMR Biomed 2011;24:1343-1352.
16
17
18
19
20
21 28. Imai H, Matsumoto H, Miyakoshi E, Okumura S, Fujiwara H, Kimura A. Regional
22 fractional ventilation mapping in spontaneously breathing mice using
23 hyperpolarized ^{129}Xe MRI. NMR Biomed 2015;28:24-29.
24
25
26
27
28
29 29. Hamedani H, Clapp JT, Kadlecck SJ, Emami K, Ishii M, Geftter WB, Xin Y, Cereda
30 M, Shaghghi H, Siddiqui S, Rossman MD, Rizi RR. Regional Fractional
31 Ventilation by Using Multibreath Wash-in ^3He MR Imaging. Radiology
32 2016;279(3):917-924.
33
34
35
36
37
38 30. Ruppert K, Brookeman JR, Hagspiel KD, Mugler JP, III. Probing lung physiology
39 with xenon polarization transfer contrast (XTC). Magn Reson Med
40 2000;44(3):349-357.
41
42
43
44 31. Imai H, Kimura A, Iguchi S, Hori Y, Masuda S, Fujiwara H. Non-invasive
45 Detection of Pulmonary Tissue Destruction in a Mouse Model of Emphysema Using
46 Hyperpolarized ^{129}Xe MRS under Spontaneous Respiration. Magn Reson Med
47 2010;64(4):929-938.
48
49
50
51
52
53 32. Hardaker EL, Freeman MS, Dale N, Bahra P, Raza F, Banner KH, Poll C. Exposing
54 rodents to a combination of tobacco smoke and lipopolysaccharide results in an
55 exaggerated inflammatory response in the lung. Br J Pharmacol
56
57
58
59
60

- 1
2
3 2010;160(8):1985-1996.
4
5
6 33. Song HH, Shin IS, Woo SY, Lee SU, Sung MH, Ryu HW, Kim DY, Ahn KS, Lee
7
8 HK, Lee D, Oh SR. Piscroside C, a novel iridoid glycoside isolated from
9
10 Pseudolysimachion rotundum var. subinegrum suppresses airway inflammation
11
12 induced by cigarette smoke. *J Ethnopharmacol* 2015;170:20-27.
13
14 34. Dregely I, Mugler JP, III, Ruset IC, Altes TA, Mata JF, Miller GW, Ketel J, Ketel S,
15
16 Distelbrink J, Hersman FW, Ruppert K. Hyperpolarized Xenon-129 gas-exchange
17
18 imaging of lung microstructure: first case studies in subjects with obstructive lung
19
20 disease. *J Magn Reson Imag* 2011;33(5):1052-1062.
21
22 35. Kirby M, Svenningsen S, Owangi A, Wheatley A, Farag A, Ouriadov A, Santyr GE,
23
24 Etemad-Rezai R, Coxson HO, McCormack DG, Parraga G. Hyperpolarized ^3He and
25
26 ^{129}Xe MR Imaging in Healthy Volunteers and Patients with Chronic Obstructive
27
28 Pulmonary Disease. *Radiology* 2012;265(2):600-610.
29
30 36. Churg A, Cosio M, Wright JL. Mechanisms of cigarette smoke-induced COPD:
31
32 insights from animal models. *Am J Physiol Lung Cell Mol Physiol*
33
34 2008;294(4):L612-631.
35
36 37. Beckett EL, Stevens RL, Jarnicki AG, et al. A new short-term mouse model of
37
38 chronic obstructive pulmonary disease identifies a role for mast cell tryptase in
39
40 pathogenesis. *J Allergy Clin Immunol* 2013;131(3):752-762.
41
42
43
44
45
46
47
48
49
50
51
52
53
54
55
56
57
58
59
60

1
2
3
4
5
6
7
8
9
10
11
12
13
14
15
16
17
18
19
20
21
22
23
24
25
26
27
28
29
30
31
32
33
34
35
36
37
38
39
40
41
42
43
44
45
46
47
48
49
50
51
52
53
54
55
56
57
58
59
60

Figure legends:

Figure 1. Example parametric maps of r_a derived from longitudinal studies of mice in each of the three groups, from top to bottom: sham-instilled; CS and LPS model of COPD; EP-treated. In all cases, the time course is shown horizontally.

Figure 2. Example parametric maps of f_D derived from longitudinal studies of mice in each of the three groups, from top to bottom: sham-instilled; CS and LPS model of COPD; EP-treated. In all cases, the time course is shown horizontally.

Figure 3. Box plots of the temporal change of mean r_a values for all mice, separated by group. Significant differences between groups are indicated by solid lines, along with the corresponding p values of significance (* $P < 0.05$; ** $P < 0.01$).

Figure 4. Box plots of the temporal change of mean f_D values for all mice, separated by group. Significant differences between groups are indicated by solid lines, along with the corresponding p values of significance (* $P < 0.05$; ** $P < 0.01$).

Figure 5. a) Box plots showing the mean MLI values obtained from mice in each of the four groups, from left to right: sham-instilled; histological analysis (CS&LPS 4w), CS and LPS model of COPD (CS&LPS10w); EP-treated. b) Representative examples of

1
2
3
4 H&E stained histology slides obtained from 5 lung regions of one mouse chosen from
5 each of the four groups. RU, right upper lobe; RM, right middle lobe; RL, right lower
6 lobe; LU, upper region of the left lobe; LL, lower region of the left lobe. Note: mean
7 values in a) represent the mean of the whole group; mean values in b) represent the
8 mean for the selected mouse from each group.
9
10
11
12
13

14
15
16
17 Figure 6. a) Box plots showing the mean bronchial wall thickness (h) values obtained
18 from mice in each of the four groups, from left to right: sham-instilled; histological
19 analysis (CS&LPS 4w), CS and LPS model of COPD (CS&LPS10w); EP-treated after
20 the 10 week experimental protocol. b) Representative examples of H&E stained
21 histology slides obtained from the four groups.
22
23
24
25
26
27
28
29

30
31 Figure 7. Relationships between HPXe MRI-derived parameters of pulmonary function
32 (r_a and f_D), and histology-derived parameters of lung structure (MLI and h) obtained
33 from the sham-instilled (\square), EP-treated (\circ), and CS and LPS (\blacktriangle) mice after the 10
34 week experimental protocol. The Pearson's r value and P value of statistical
35 significance are noted in each plot.
36
37
38
39
40
41
42
43
44
45
46
47
48
49
50
51
52
53
54
55
56
57
58
59
60

1
2
3 Supporting Figure S1. a) Box plots showing the mean bronchial wall thickness (h)
4 values obtained from mice in each of the five groups, from left to right:
5 sham-instilled; histological analysis (CS&LPS 4w and CS&LPS 6w), CS and LPS
6 model of COPD (CS&LPS10w); EP-treated after the 10 week experimental protocol. b)
7
8 Representative examples of H&E stained histology slides obtained from the five
9
10
11
12
13
14
15
16
17
18
19
20
21
22
23
24
25
26
27
28
29
30
31
32
33
34
35
36
37
38
39
40
41
42
43
44
45
46
47
48
49
50
51
52
53
54
55
56
57
58
59
60

For Peer Review

1
2
3
4
5
6
7 **Treatment response of ethyl pyruvate in a mouse model of chronic obstructive**
8 **pulmonary disease studied by hyperpolarized ^{129}Xe MRI**

9
10 Atsuomi Kimura,*¹ Yukiko Yamauchi,¹ Shota Hodono,¹ Neil James Stewart,² Osamu
11
12 Hosokawa,¹ Yu Hagiwara,¹ Hirohiko Imai,³ and Hideaki Fujiwara¹
13
14

15
16
17 ¹ Department of Medical Physics and Engineering, Division of Medical Technology
18 and Science, Faculty of Health Science, Graduate School of Medicine, Osaka
19 University
20
21

22 ² Academic Unit of Radiology, University of Sheffield, Sheffield, South Yorkshire, UK
23

24 ³ Research and Educational Unit of Leaders for Integrated Medical System, Center for
25 the Promotion of Interdisciplinary Education and Research, Kyoto University, Kyoto,
26
27 Japan
28
29

30
31
32 Running head:

33
34 HPXe MRI of murine COPD model and therapy response
35
36

37
38 Word count: 4492
39
40

41
42 *Corresponding author: Atsuomi Kimura, PhD, Department of Medical Physics and
43 Engineering, Division of Medical Technology and Science, Faculty of Health Science,
44 Graduate School of Medicine, Osaka University, 1-7 Yamadaoka, Suita, Osaka
45
46 565-0871, Japan,
47
48

49
50 Phone: +81-6-6879-2478, E-mail: kimura@sahs.med.osaka-u.ac.jp
51
52

ABSTRACT

Purpose: To investigate disease progression and treatment response in a murine model of chronic obstructive pulmonary disease (COPD) using a preclinical hyperpolarized ^{129}Xe (HPXe) MRI strategy.

Methods: COPD phenotypes were induced in 32 mice by 10 weeks of exposure to cigarette smoke (CS) and lipopolysaccharide (LPS). The efficacy of ethyl pyruvate (EP), an anti-inflammatory drug, was investigated by administering EP to 16 of the 32 mice after 6 weeks of CS and LPS exposure. HPXe MRI was performed to monitor changes in pulmonary function during disease progression and pharmacological therapy.

Results: HPXe metrics of fractional ventilation and gas-exchange function were significantly reduced after 6 weeks of CS and LPS exposure compared to sham-instilled mice administered with saline ($P < 0.05$). After this observation, EP administration was started in 16 of the 32 mice and continued for 4 weeks. EP was found to improve HPXe MRI metrics to a similar level as in sham-instilled mice ($P < 0.01$). Histological analysis showed significant alveolar tissue destruction in the COPD group, but relatively normal alveolar structure in the EP and sham-instilled groups.

Conclusion: This study demonstrates the potential efficacy of EP for COPD therapy, as assessed by a non-invasive, translatable ^{129}Xe MRI procedure.

Abstract word count: 200

Keywords: Hyperpolarized ^{129}Xe MRI, lung functional assessment, murine chronic obstructive pulmonary disease, treatment response, ethyl pyruvate

Comment [XH1]: R1.6

Comment [XH2]: R1.7

Comment [XH3]: R1.8

Comment [XH4]: R1.9

INTRODUCTION

Chronic obstructive pulmonary disease (COPD), a heterogeneous lung disease characterized by both chronic airway inflammation and emphysematous alveolar tissue destruction, is predicted to be the third leading cause of death worldwide by 2020 (1).

At present, pharmacological therapies for COPD have shown limited efficacy and thus the development of new therapeutic drugs is vital for improving patient outcomes (2).

The use of appropriate animal models of COPD that adequately induce the key symptoms of the disease is indispensable for therapy development, and rodent models are especially important. In particular, preclinical studies with mice are often appropriate because a wide range of well-characterized disease models are available (3,4). As smoking and repeated lung infections are the primary causes of COPD, several murine COPD models have been developed by exposing mice to cigarette smoke. Despite certain models showing good reproducibility for inducing the two main phenotypes of COPD mentioned above, the lack of applicable methods for assessment and diagnosis of these disease models remains a limiting factor for preclinical studies. Most previous studies have relied on plethysmography and/or histology to evaluate the applicability of murine COPD models, necessitating a tracheostomy and/or mouse death for each examination (5,6) and hence making it difficult to evaluate drug efficacy repetitively and longitudinally. To help resolve this problem, non-invasive imaging techniques that allow the longitudinal assessment of disease progression and therapeutic efficacy of drugs in vivo are required.

MRI using hyperpolarized (HP) noble gases (^3He and ^{129}Xe) as contrast agents offers an attractive means to visualize and quantitatively evaluate pulmonary functional parameters such as ventilation and gas-exchange (7-9). In a number of studies in small animals and humans, pathological changes of these fundamental

1
2
3
4
5
6
7 parameters have been investigated using HP gas MRI and quantitative measures of
8 ventilation and gas-exchange dysfunction caused by COPD have been established
9 (10,11). HP ^{129}Xe (HPXe) is a versatile contrast agent to evaluate drug efficacy in the
10 lungs because it allows not only imaging of ventilation, but also the assessment of
11 pulmonary gas-exchange, thanks to its solubility in pulmonary tissues and blood. To
12 this end, we have developed a continuous-flow mode polarizer for HPXe production
13 and have established non-invasive MRI procedures under spontaneous respiration for
14 the assessment of pulmonary function in mice (12,13). In this study, we apply our
15 HPXe methodology to explore the feasibility of a new drug for COPD therapy.

Comment [XH6]: R1.15

16
17
18
19
20
21
22
23
24
25 Ethyl pyruvate (EP), an anti-inflammatory agent, is a candidate for
26 pharmacological therapy of COPD. In recent years, EP has been shown to demonstrate
27 therapeutic efficacy in various animal models of lung diseases, such as acute lung
28 injury (ALI) and pulmonary arterial hypertension (PAH) (15-17). The therapeutic
29 efficacy of EP is attributed to its ability to regulate high-mobility group box protein-1
30 (HMGB1) release from innate immune cells, and to deactivate subsequent cytokine
31 production that would further stimulate inflammatory responses (18,19). HMGB1,
32 which is an abundant chromatin protein, may play a crucial role in pharmacological
33 therapy of COPD because it is known to not only trigger inflammatory responses but
34 also, paradoxically, to activate cells involved in tissue repair (20-24). HMGB1
35 functions by binding with the receptor for advanced glycation end products (RAGE)
36 and Toll-Like Receptors 2 and 4. In recent years, it has been shown that HMGB1 can
37 also initiate wound healing processes through binding with RAGE followed by
38 activation of the extracellular signal-regulated kinase 1/2 (ERK1/2) signaling pathway
39 (23). RAGE is expressed in pulmonary tissues with relatively high basal levels (22),
40 and EP has been reported to activate the ERK1/2 signaling pathway (14). Thus, EP
41
42
43
44
45
46
47
48
49
50
51
52
53
54
55
56
57
58
59
60

1
2
3
4
5
6
7 shows considerable potential as a drug for lung tissue repair accompanied with
8 anti-inflammatory responses through regulation of the HMGB1/RAGE pathway.

Comment [XH7]: R2.1

9
10
11 In the present study, we demonstrate the observation of disease progression in a
12 mouse model of COPD induced by cigarette smoke (CS) exposure and
13 lipopolysaccharide (LPS) instillation, as measured by HPXe MRI. Additionally, the
14 efficacy of ethyl pyruvate (EP) for treatment of this COPD model is studied to assess
15 the feasibility of this non-invasive imaging technique as a diagnostic method for early
16 disease detection and therapy response evaluation in COPD.
17
18
19
20
21
22
23

24 **METHODS**

25 **Animal preparation**

26
27
28 Thirty-seven male, 6-week-old, type ddY mice, weighing 30 – 35 g (Japan SLC, Inc.,
29 Shizuoka, Japan) were included in this study. All experimental procedures and animal
30 care standards conformed to Osaka University guidelines. Mice were divided into two
31 groups: a sham-instilled group of N=5 mice and a CS and LPS group of N=32. The CS
32 and LPS mice were further divided into 2 equal groups of 16 individuals. The two
33 subgroups were separately administered with a combination of CS and LPS as follows.
34 CS of approximately 2.1 L in volume resulting from one cigarette (Lark Milds: tar 9
35 mg, nicotine 0.8 mg; Philip Morris International Inc., New York, USA) was collected
36 into a Tedlar® bag (Sigma-Aldrich, St Louis, MO, USA). The mice in each subgroup
37 were placed in a semi-sealed plastic container with a volume of 12.4 L and 9 airshafts
38 of 5 mm inner diameter on its upper surface. CS was flowed from the Tedlar® bag into
39 the container for 26 minutes at a rate of 40 mL/min. Following this, fresh room air was
40 flowed into the container for 5 minutes (at 720 mL/min). This whole-body exposure
41
42
43
44
45
46
47
48
49
50
51
52
53
54

1
2
3
4
5
6
7 procedure was performed twice daily on five consecutive days within one week, and
8 repeated on a weekly basis as described below. On each fifth day, a 20 μ L solution of
9 LPS in saline (0.4 mg/kg, LPS in *Escherichia coli*, serotype O55:B5, Sigma-Aldrich,
10 St. Louis, MO, USA) was delivered intra-tracheally to the mice at least 2 hours prior
11 to the CS exposure. The sham-instilled mice were intra-tracheally administered with
12 20 μ L of saline on every fifth day in the same manner as the LPS administration.
13
14
15
16
17
18

19 Six weeks after commencing CS and LPS exposure, the two subgroups of CS and
20 LPS mice were assigned as follows: a pure CS and LPS group of N=16 mice and an
21 EP-treated group of N=16 mice. For the pure CS and LPS group, the same protocol of
22 CS and LPS administration was continued for a further 4 weeks. EP-treated mice were
23 intra-tracheally administered with a 20 μ L solution of EP in saline (1.3 mg/kg, Tokyo
24 Chemical Industry Ltd, Tokyo, Japan) on a daily basis for 4 weeks, in addition to the
25 continued administration of CS and LPS as detailed above. EP was always
26 administered after the CS and LPS exposure, separated by an interval of at least 2
27 hours. Therefore, in total, 10 weeks were required to completely prepare the CS and
28 LPS, and EP-treated groups. The sham-instilled mice were intra-tracheally
29 administered with 20 μ L of saline per day, every weekday, for this 4 week period, in
30 the same manner as the EP treatment. The survival rates of the whole 10-week
31 procedure were 75% for CS and LPS mice (12 out of 16 mice survived), 75% for
32 EP-treated mice (12 out of 16 mice survived), and 100 % for the sham-instilled group.
33
34
35
36
37
38
39
40
41
42
43
44
45
46

47 In all cases, prior to the instillation of saline, LPS or EP solution, mice were
48 anesthetized with 2% isoflurane (ISOFLU®, Dainippon Sumitomo Pharmaceutical Co.
49 Ltd, Osaka, Japan), which was administered via a nose cone using a home-built
50 anesthesia system connected to an isoflurane vaporizer (Isorex I-200, Shin-Ei
51
52
53
54

1
2
3
4
5
6
7
8
9
10
11
12
13
14
15
16
17
18
19
20
21
22
23
24
25
26
27
28
29
30
31
32
33
34
35
36
37
38
39
40
41
42
43
44
45
46
47
48
49
50
51
52
53
54
55
56
57
58
59
60

Industries, Inc., Tokyo, Japan). Subsequently, mice were intubated with a 22 G catheter (SURFLO® F&F, Terumo Corp., Tokyo, Japan) while positioned supine and secured to a slanted wooden board, and then the saline, LPS or EP solution was instilled.

MR measurements of sham-instilled and CS and LPS groups were performed at 0 weeks (prior to the first administration) and 2, 6, 8 and 10 weeks after commencing the administration of CS and LPS. Similarly, MR measurements of the EP-treated group were performed at 0, 6, 8 and 10 weeks after commencing the administration of CS and LPS (i.e. -6, 0, 2 and 4 weeks from commencement of EP therapy). Immediately before all MR measurements, mice were anesthetized with 2 % isoflurane as detailed above. A plastic mouth mask, to which three polyethylene tubes were connected (for HPXe gas delivery, O₂ delivery and exhaled gas exhaust), was attached to the animal prior to placement in the MR scanner. In order to synchronize image acquisitions with respiratory motion, a pulse transducer (AD Instruments Ltd., Dunedin, New Zealand) was positioned on the mouse abdomen, just inferior to the diaphragm. This sensor converted the respiratory motion into an electrical signal that was monitored in real-time using LabVIEW software (National Instruments, Austin, TX, USA). The animal's body temperature in the magnet was maintained with warm water circulating through a rubber tube placed on the abdomen. The MR imaging procedure was performed without tracheal intubation or tracheotomy and hence was entirely non-invasive.

¹²⁹Xe Polarization and Gas Delivery

¹²⁹Xe nuclei were polarized to ~10% by Rb-¹²⁹Xe spin-exchange optical pumping (25) with a home-built continuous-flow ¹²⁹Xe polarizer (26). A gas mixture consisting of 70% Xe (natural abundance, comprising 26% ¹²⁹Xe) and 30% N₂ was supplied from a pre-mixed cylinder (Air Liquid Japan Ltd., Tokyo, Japan) at a pressure of 0.15 atmospheres for ¹²⁹Xe polarization. Once polarized, HPXe was subsequently compressed to atmospheric pressure with a diaphragm pump (LABOPORT® N86 KN.18, KNF Neuberger GmbH, Freiburg, Germany) to facilitate gas delivery directly and continuously from the polarizing cell to the mouse in the magnet. The HPXe gas mixture was flowed continuously at a rate of 50 mL/min to each mouse and was mixed with O₂ (continuously supplied at 9 mL/min) in the mouth mask. The percentages of Xe and O₂ spontaneously inhaled by the mice were 59.3% and 15.3%, respectively.

MR Imaging

All MR measurements were performed on a Varian Unity INOVA 400 WB high-resolution NMR spectrometer system running VNMR 6.1C software (Varian Inc., Palo Alto, CA, USA). A 9.4 T vertical magnet with a bore width of 89 mm (Oxford Instruments Plc., Oxford, UK) was used. A self-shielded gradient probe was employed in combination with Litz volume RF coils of 34 mm inner diameter, tunable to the Larmor frequencies of ¹²⁹Xe (110.6 MHz) and ¹H (399.6 MHz) (Clear Bore DSI-1117, Doty Scientific, Inc., Columbia, SC, USA).

For assessment of pulmonary ventilation and gas-exchange function, HPXe gas images were acquired with a 2D multi-shot balanced steady-state free precession (bSSFP) sequence, which was programmed in-house (27). Acquisition parameters were as follows: RF pulse, 1000 μs long Gaussian-shaped pulse with a bandwidth of 2800 Hz and centered on the ¹²⁹Xe gas-phase resonance (0 ppm); TR/TE, 3.2/1.6 ms;

1
2
3
4
5
6
7 receiver bandwidth, 62 kHz; one coronal slice of thickness 20 mm, covering the whole
8 of the lungs; matrix size, 64×32 ; field of view, $80 \times 25.6 \text{ mm}^2$; number of shots
9 (required to fill k-space), 4; flip angle, 40° ; number of averages of the whole
10 acquisition, 8; centrically-ordered phase encoding. ^{129}Xe images were reconstructed
11 by a 2D fast Fourier transform after zero filling to a 128×64 matrix using in-house
12 MATLAB scripts (MathWorks Inc., Natick, MA, USA).
13
14
15
16
17
18
19
20

Comment [XH8]: R1.16

21 Evaluation of ventilation function

22 For evaluating pulmonary ventilation function, the fractional ventilation (i.e. the
23 fraction of gas “turned over” per breathing cycle), r_a , was mapped across the lungs
24 following a previously reported method (28,29). Briefly, after the HPXe concentration
25 in the lungs had reached a steady-state under the continuous supply of HPXe and O_2 ,
26 two pre-saturation RF pulses were applied at the ^{129}Xe gas-phase frequency to destroy
27 any gas-phase ^{129}Xe magnetization in the alveoli. The bSSFP imaging sequence was
28 then used to acquire respiratory-synchronized ^{129}Xe gas ventilation images at
29 inspiration after n breathing cycles. The value of n was sequentially incremented from
30 1 to 10, and then to 12, 15 and 20; thus, thirteen ^{129}Xe ventilation images were
31 acquired in total. (In Reference (28), images were acquired after 1 to 10 breaths only;
32 the purpose of the additional acquired images here was to improve the accuracy of the
33 r_a estimate.) From the resulting image series, the fractional ventilation of each voxel
34 was evaluated by analyzing the dependency of the ^{129}Xe MR signal intensity upon the
35 number of breaths (Equations 2 and 3, Reference (28)). The fractional ventilation, r_a ,
36 is defined as:
37
38
39
40
41
42
43
44
45
46
47
48
49
50

Comment [XH9]: R1.18

Comment [XH10]: R1.19

$$r_a = \frac{V_f}{V_o + V_f}, \quad [1]$$

52
53
54
55
56
57
58
59
60

where V_o and V_f denote the volumes of old and new (fresh) gas within the voxel after each breath, respectively. r_a values were determined pixel-by-pixel over the whole image to derive a r_a map, and averaged for each mouse to obtain the whole lung r_a . Finally, the whole lung r_a values were averaged for each of the sham-instilled, CS and LPS, and EP-treated groups to obtain group mean r_a values.

Evaluation of gas-exchange function

The efficiency of HPXe gas-exchange between the alveoli (gas-phase) and the lung parenchyma and capillaries (dissolved-phase) was evaluated by the xenon polarization transfer contrast (XTC) method (30). Briefly, a XTC image was generated by acquiring bSSFP gas ventilation images at expiration, separated by the application of four frequency-selective inversion pulses (inter-pulse delay 20 ms) at the Larmor frequency of dissolved-phase ^{129}Xe (197 ppm), and comparing the resulting ventilation image intensities (27). The flip angle of the inversion pulse (Gaussian-shape; 1000 μs duration) was calibrated prior to the present study. Similarly, a “control” bSSFP image was generated by acquiring ventilation images at expiration, separated by the application of the same inversion pulses, but centered at -197 ppm instead of 197 ppm. The whole XTC measurement was repeated three times, and the three images were summed to improve image SNR. The parameter of gas-exchange function, f_D , defined as the fractional depolarization of gas-phase HPXe caused by the repeated RF inversion of dissolved-phase HPXe during continuous diffusive exchange of xenon between the two compartments, was calculated according to the ratio of the signal intensities of control and XTC images as follows:

$$f_D(\%) = \left(1 - \sqrt[N]{\frac{S_{XTC}}{S_{control}}}\right) \times 100 \quad [2]$$

where S_{XTC} and $S_{control}$ are the signal intensities of XTC and control images,

Comment [XH11]: R1.1

Comment [XH12]: R1.20

Comment [XH13]: R1.1

1
2
3
4
5
6
7 respectively, and N is the number of inversion pulses. f_D values were calculated on a
8 pixel-by-pixel basis in order to create a whole lung f_D map. As with the r_a analysis,
9 mean f_D values were obtained for each of the sham-instilled, CS and LPS, and
10 EP-treated groups.
11
12
13

14
15
16
17 For each of the above described techniques, the existence of statistically-significant
18 differences in mean values of derived parameters between groups was assessed by the
19 analysis of variance (ANOVA) method with the Tukey-Kramer test, using the JMP
20 Statistics package (SAS Institute Inc., Cary, NC, USA).
21
22
23

24 25 26 27 **Histological Analysis**

28 After completion of the MR experiments (week 10), the mice were euthanized with a
29 lethal dose of carbon dioxide gas. Lungs were extracted and fixed in a 10 % formalin
30 solution, and hematoxylin and eosin (H&E) stained slides were created to analyze
31 morphological changes to the alveoli and terminal bronchioles. Four slides per mouse
32 were used to evaluate structural parameters including mean linear intercept (MLI) and
33 mean bronchial wall thickness (h), as previously described (31). Five MLI and h
34 values were calculated from each slide, corresponding to the five lobar regions of the
35 lung (right upper lobe, right middle lobe and right lower lobe; left upper lobe and left
36 lower lobe). Each set of five values was averaged over the four slides, and then the
37 resulting five averaged regional MLI and h values were in turn averaged to yield a
38 single MLI and h value for each mouse. Mean MLI and h values were calculated for
39 each of the sham-instilled, CS and LPS, and EP-treated groups in this manner.
40
41
42
43
44
45
46
47
48
49
50
51

52 In order to monitor morphological changes during the 10 weeks of CS and LPS
53 administration, one additional CS and LPS histological analysis group (N=3 mice) was
54
55

Comment [XH14]: R1.21&22

1
2
3
4
5
6
7 prepared after 4 weeks of administration using the same protocol as described above.

8
9 MLI and h values were evaluated for these groups as described above.

10 11 12 13 RESULTS

14
15 Figures 1 and 2 show the longitudinal changes in r_a and f_D maps, respectively, after 0,
16
17 6, 8 and 10 weeks of CS and LPS administration, for one representative mouse from
18
19 each of the sham-instilled, CS and LPS, and EP-treated groups. [It should be noted that
20
21 Figures 1 and 2 were additionally processed with a 2 x 2 median filter using ImageJ
22
23 (National Institute of Health) to reduce the prevalence of artifacts associated with
24
25 cardiac motion and rapid diffusion of HPXe in the major airways. These maps depict
26
27 the regional variation in pulmonary ventilation and gas-exchange functional changes
28
29 over time. In particular, they highlight an approximately spatially homogeneous
30
31 reduction of r_a in the CS and LPS mice after 10 weeks, and an overall improvement in
32
33 r_a and f_D in response to EP therapy, with some regional heterogeneity.

34
35 Figures 3 and 4 display the group-mean values of r_a and f_D , respectively, after 0,
36
37 2, 6, 8 and 10 weeks of CS and LPS exposure. The mean r_a value for the CS and LPS
38
39 group was found to be significantly decreased compared to that of the sham-instilled
40
41 group after 6 weeks ($P < 0.05$), and was observed to continue to decrease for the
42
43 remainder of the 10 week measurement period (after 10 weeks, $r_{a,CS\&LPS} = 0.19 \pm 0.03$,
44
45 compared with $r_{a,Sham-instilled} = 0.25 \pm 0.03$, $P < 0.01$). The mean r_a value of the EP
46
47 group was comparable to that of the sham-instilled mice ($r_{a,EP} = 0.25 \pm 0.03$) after 10
48
49 weeks, i.e. 4 weeks of EP administration. This value is also significantly larger than
50
51 that of the CS and LPS group; $P < 0.01$. The f_D value of the CS and LPS group
52
53 ($f_{D,CS\&LPS} = 4.5 \pm 1.1$ %) was significantly lower ($P < 0.01$) than that of the
54
55 sham-instilled group ($f_{D,Sham-instilled} = 6.8 \pm 0.6$ %) after 10 weeks of exposure to CS

56
57
58
59
60
12

Comment [XH15]: R1.2

1
2
3
4
5
6
7
8
9
10
11
12
13
14
15
16
17
18
19
20
21
22
23
24
25
26
27
28
29
30
31
32
33
34
35
36
37
38
39
40
41
42
43
44
45
46
47
48
49
50
51
52
53
54
55
56
57
58
59
60

and LPS, while the f_D value of the EP group was considerably improved ($f_{D,EP} = 6.2 \pm 0.9$ %) compared with that of the CS and LPS group ($P < 0.01$). The longitudinal variation in mean r_a and f_D values from all groups was found to correlate significantly (Pearson's $r = 0.820$, $P < 0.01$).

Figures 5 and 6 depict whole lung mean MLI and h values and representative histological images obtained from mice from each of the sham-instilled, EP-treated and CS and LPS groups at the end of the 10 week experimental protocol, and the histological analysis group, respectively. As illustrated in these figures, an enlargement of the alveolar airspace volume was observed at week 10 following bronchial wall thickening; this is discussed below. The mean MLI of the CS and LPS group ($MLI_{CS\&LPS} = 44.0 \pm 3.8$ μm) was significantly larger than that of the sham-instilled group ($MLI_{Sham-instilled} = 39.7 \pm 1.8$ μm , $P < 0.05$). The mean MLI of the EP-treated group ($MLI_{EP} = 38.2 \pm 2.4$ μm) was smaller than that of the CS and LPS group ($P < 0.01$) and similar to that of the sham-instilled group. The h value of the EP-treated group ($h_{EP} = 12.5 \pm 1.1$ μm) was smaller than that of the CS and LPS group ($h_{CS\&LPS} = 14.9 \pm 1.3$ μm , $P < 0.01$), and similar to that of the sham-instilled group ($h_{Sham-instilled} = 12.3 \pm 0.6$ μm) at week 10. Meanwhile, the mean MLI and h values of the histological analysis group (exposed to CS and LPS for 4 weeks) were $MLI_{HA_4w} = 39.8 \pm 2.5$ μm and $h_{HA_4w} = 14.1 \pm 0.6$ μm , respectively, which were comparable to those of the sham-instilled mice.

Figure 7 shows correlation plots of individual r_a , f_D , h and MLI values obtained from the sham-instilled, EP-treated and CS and LPS mice after the 10 week experimental protocol. Significant positive correlations were observed between r_a and f_D , and MLI and h , as were significant negative correlations between r_a and h , f_D and h , and f_D and MLI ($P < 0.05$). The correlation between r_a and MLI was not statistically

1
2
3
4
5
6
7 significant ($P > 0.05$).
8
9

10 11 **DISCUSSION**

12
13 In the present study, a murine model of COPD was developed by 10 weeks of exposure
14 to CS and LPS, and the associated induced temporal changes of pulmonary ventilation
15 and gas-exchange function were assessed noninvasively by HPXe MRI. The present
16 COPD model was able to induce characteristic emphysematous alveolar tissue
17 destruction, achieved by modifying previous protocols for producing airway
18 inflammation using CS and LPS (21,32,33). The longitudinal HPXe MRI assessment of
19 pulmonary function revealed a significant decrease in parameters of both fractional
20 ventilation, r_a , and gas-exchange, f_D , of the CS and LPS mice after 6 weeks of CS and
21 LPS exposure. However, for the first 2 weeks, pulmonary function in these mice was
22 not notably different from that of sham-instilled mice. The longitudinal variation in
23 the mean values of the two parameters was found to correlate, suggesting that the
24 time-course of disease progression acted to simultaneously impair both ventilation and
25 gas-exchange function. In addition, the r_a and f_D values were found to correlate
26 significantly on a per mouse basis at week 10, although not prior to week 10, which
27 supports the decision to end the CS and LPS administration at this time-point.
28 Reductions in f_D and increases in the prevalence of ventilation defects have been
29 previously observed using hyperpolarized gas MRI in human COPD patients (34,35),
30 supporting the fact that the CS and LPS model of COPD employed here could
31 successfully induce similar pathological effects to COPD itself. Combining
32 whole-body CS exposure with LPS administration induced significant emphysematous
33 pathology and bronchial wall thickening after 10 weeks of exposure, as illustrated by
34 histology slides (Figures 5 and 6). On the other hand, exposure to only CS has been
35
36
37
38
39
40
41
42
43
44
45
46
47
48
49
50
51
52
53
54
55
56
57
58
59
60

Comment [XH16]: R2.2

Comment [XH17]: R1.23&24

1
2
3
4
5
6
7 reported to typically require ≥ 6 months to establish the characteristic emphysematous
8 pathology in mice (36). While Hansbro et al. succeeded to establish a mouse model of
9 COPD by 8 weeks of CS exposure through the nose only, this procedure required
10 purpose-built equipment that is not readily translatable to our laboratory, and the CS
11 dose was relatively high (2 cigarettes/mouse/day) (37). Thus, our protocol of CS and
12 LPS exposure considerably shortened the time required to produce the two phenotypes
13 of COPD pathology without necessitating specialist equipment. As such, this
14 procedure may be advantageous for future investigations of COPD treatment response.

Comment [XH18]: R1.25

15
16
17
18
19
20
21
22
23 The present COPD mouse model caused significant decreases of ventilation and
24 gas-exchange parameters: mean r_a of 0.19 ± 0.03 in CS and LPS mice compared with
25 0.25 ± 0.03 in sham-instilled mice; mean f_D of $4.5 \pm 1.0\%$ compared with $6.8 \pm 0.6\%$,
26 respectively, after 10 weeks. The decrease of r_a after 10 weeks of exposure to CS and
27 LPS is indicative of an increase in the bronchial wall thickness, and indeed r_a showed
28 a significant correlation with the histology-derived h value at this time-point (Figure
29 7). However, the decrease of f_D is indicative of both a reduction in the volume of
30 septal tissue and an increase in the bronchial wall thickness. The decrease in f_D and r_a
31 at the 6 week time-point may be attributable to the increase in bronchial wall thickness,
32 h , (see Supporting Figure S1) since it is unlikely that the volume of septal tissue
33 decreased (as there was no significant change in MLI at the 4 week time-point). This
34 situation may be similar to a previous study in which CS and LPS were administered to
35 rats for 6 weeks (21). According to that report, no histological evidence of COPD (i.e.
36 MLI change) was seen despite overexpression of HMGB1. However, it is worth noting
37 that these observations might not exclude the possibility of early stage emphysema,
38 because mice lack the anatomical characteristics (respiratory bronchioles) for
39 expression of centrilobular emphysema (4). One might also expect that the decrease in
40
41
42
43
44
45
46
47
48
49
50
51
52
53
54
55

Comment [XH19]: R2.2

Comment [XH20]: R1.26

Comment [XH21]: R1.28

f_D was caused in part by a reduction in the volume of the pulmonary capillaries, because the f_D measurement includes a contribution related to blood volume (since ddY-type mice exhibit only a single NMR peak from dissolved-phase ^{129}Xe in lung tissue and blood (31), and furthermore, the XTC technique as employed herein does not enable the distinction of two dissolved-phase ^{129}Xe compartments even if they were present).

In the present study, the efficacy of EP for treatment of the CS and LPS model of COPD was quantified by longitudinal observations of pulmonary function. The reductions in r_a and f_D in the CS and LPS group after 6 weeks recovered to a similar level as the sham-instilled group by 2 and 4 weeks of administration of EP, respectively ($P < 0.01$, see Figures 3 and 4). Because the administration of EP was only started 6 weeks after commencement of CS and LPS exposure (i.e. after some impairment of pulmonary function was observed), EP likely exhibited a combination of both preventative and therapeutic properties in the CS and LPS model of COPD. In other words, EP may have acted to inhibit further emphysema development and to repair the existing bronchial wall damage (Figures 5 and 6). This hypothesis is supported by the lack of significant difference in the r_a and f_D values between 6 and 10 week time-points in the EP-treated group ($P > 0.05$). However, the present study was unable to clarify whether the recovery of HPXe MRI metrics might be indicative of the reparation of tissue loss by early emphysema and/or improved pulmonary hemodynamics. To prove whether EP can indeed act to reverse emphysematous tissue loss, further experiments are needed in which EP administration is started after 10 weeks of CS and LPS exposure.

To the best of our knowledge, this is the first evidence of the therapeutic action of EP in a murine COPD model, as measured by HPXe MRI. Recently, it has been

Comment [XH22]: Reply to

editor

R1.3&5

R2.0

Comment [XH23]: R1.29

Comment [XH24]: R2.11

Comment [XH25]: R1.30

1
2
3
4
5
6
7 reported that intraperitoneal administration of EP can inhibit the expression of
8
9 HMGB1 (18,19). Additionally, high expression of HMGB1 has been reported to lead to
10
11 lung functional impairment, and is associated with the development and progression of
12
13 COPD (20-22). On the other hand, albeit paradoxically, the HMGB1/RAGE pathway is
14
15 also known to be associated with a series of signalling pathways for tissue repair
16
17 (23,24). It may be speculated that EP is effective in treating lung diseases caused by
18
19 chronic inflammation (such as the CS and LPS model of COPD) through the regulation
20
21 of HMGB1/RAGE, leading to improvement and potentially maintenance of murine
22
23 pulmonary function. Further studies with corresponding molecular assays are required
24
25 to substantiate this claim.
26
27

28 **CONCLUSION**

29
30 The feasibility of HPXe MRI for longitudinal assessment of disease progression and
31
32 pharmacological therapy has been demonstrated in a mouse model of COPD. The
33
34 model, combining exposure to cigarette smoke and lipopolysaccharide solution,
35
36 induced COPD characteristics in mice in a relatively short time of 10 weeks and offers
37
38 potential advantages for pharmacological therapy assessment applications. HPXe
39
40 MRI-derived metrics of pulmonary function showed considerable impairment in both
41
42 ventilation and gas-exchange function in CS and LPS mice compared with
43
44 sham-instilled mice, as verified by histological analysis. Longitudinal HPXe MRI
45
46 assessment of the action of an anti-inflammatory agent, ethyl pyruvate, for treatment
47
48 of this COPD model revealed preliminary evidence of its efficacy, and may help to
49
50 elucidate the exact mechanisms of its therapeutic action in the future.
51
52
53
54
55
56
57
58
59
60

Comment [XH26]: R1.31

Comment [XH27]: R2.12

1
2
3
4
5
6
7 Acknowledgements

8
9 This work was supported by the Japan Society for the Promotion of Science (JSPS)
10
11 KAKENHI grant numbers: JP24300163 and JP15H03006. NJS acknowledges funding
12
13 support from the Medical Research Council (MRC) and the JSPS summer programme
14
15 (2015).
16
17
18
19
20
21
22
23
24
25
26
27
28
29
30
31
32
33
34
35
36
37
38
39
40
41
42
43
44
45
46
47
48
49
50
51
52
53
54

1
2
3
4
5
6
7
8
9
10
11
12
13
14
15
16
17
18
19
20
21
22
23
24
25
26
27
28
29
30
31
32
33
34
35
36
37
38
39
40
41
42
43
44
45
46
47
48
49
50
51
52
53
54
55
56
57
58
59
60

References

1. Lozano R, Naghavi M, Foreman K, et al. Global and regional mortality from 235 causes of death for 20 age groups in 1990 and 2010: a systematic analysis for the Global Burden of Disease Study 2010. *The Lancet* 2012;380(9859):2095-2128.
2. Holgate S, Agusti A, Strieter RM, Anderson GP, Fogel R, Bel E, Martin TR, Reiss TF. Drug development for airway diseases: looking forward. *Nat Rev Drug Discov* 2015;14:367-368.
3. Fricker M, Deane A, Hansbro PM. Animal models of chronic obstructive pulmonary disease. *Expert Opin Drug Discov* 2014;9(6):629-645.
4. Gardi C, Stringa B, Martorana PA. Animal models for anti-emphysema drug discovery. *Expert Opin Drug Discov* 2015;10(4):399-410.
5. Mizutani N, Fuchikami J, Takahashi M, Nabe T, Yoshino S, Kohno S. Pulmonary emphysema induced by cigarette smoke solution and lipopolysaccharide in guinea pigs. *Biol Pharm Bull* 2009;32:1559-1564.
6. Li JJ, Wang W, Baines KJ, Bowden NA, Hansbro PM, Gibson PG, Kumar RK, Foster PS, Yang M. IL-27/IFN- γ induce MyD88-dependent steroid-resistant airway hyperresponsiveness by inhibiting glucocorticoid signaling in macrophages. *J Immunol* 2010;185(7):4401-4409.
7. Fain SB, Korosec FR, Holmes JH, O'Halloran R, Sorkness RL, Grist TM. Functional lung imaging using hyperpolarized gas MRI. *J Magn Reson Imag* 2007;25(5):910-923.
8. Mugler JP, III, Altes TA. Hyperpolarized ^{129}Xe MRI of the human lung. *J Magn Reson Imag* 2013;37(2):313-331.
9. van Beek EJR, Wild JM, Kauczor H-U, Schreiber W, Mugler JP, de Lange EE. Functional MRI of the lung using hyperpolarized 3-helium gas. *J Magn Reson Imag*

- 2004;20(4):540-554.
10. Kirby M, Pike D, Coxson HO, McCormack DG, Parraga G. Hyperpolarized ^3He ventilation defects used to predict pulmonary exacerbations in mild to moderate chronic obstructive pulmonary disease. *Radiology* 2014;273(3):887-896.
 11. Qing K, Mugler JP 3rd, Altes TA, Jiang Y, Mata JF, Miller GW, Ruset IC, Hersman FW, Ruppert K. Assessment of lung function in asthma and COPD using hyperpolarized ^{129}Xe chemical shift saturation recovery spectroscopy and dissolved-phase MRI. *NMR Biomed* 2014;27(12):1490-1501.
 12. Imai H, Kimura A, Fujiwara H. Small animal imaging with hyperpolarized ^{129}Xe magnetic resonance. *Anal Sci* 2014;30(1):157-166.
 13. Tetsumoto S, Takeda Y, Imai H, et al. Validation of noninvasive morphological and diffusion imaging in mouse emphysema by micro-computed tomography and hyperpolarized ^{129}Xe magnetic resonance imaging. *Am J Respir Cell Mol Biol* 2013;49(4):592-600.
 14. Kung CW, Lee YM, Cheng PY, Peng YJ, Yen MH. Ethyl pyruvate reduces acute lung injury via regulation of iNOS and HO-1 expression in endotoxemic rats. *J Surg Res* 2011;167(2):e323-e331.
 15. Liu C, Fang C, Cao G, Liu K, Wang B, Wan Z, Li S, Wu S. Ethyl pyruvate ameliorates monocrotaline-induced pulmonary arterial hypertension in rats. *J Cardiovasc Pharmacol* 2014;64(1):7-15.
 16. Shang GH, Lin DJ, Xiao W, Jia CQ, Li Y, Wang AH, Dong L. Ethyl pyruvate reduces mortality in an endotoxin-induced severe acute lung injury mouse model. *Respir Res* 2009;10:91.
 17. Pulathan Z, Altun G, Hemşinli D, Menteşe A, Yuluğ E, Civelek A. Role of ethyl pyruvate in systemic inflammatory response and lung injury in an experimental

1
2
3
4
5
6
7
8
9
10
11
12
13
14
15
16
17
18
19
20
21
22
23
24
25
26
27
28
29
30
31
32
33
34
35
36
37
38
39
40
41
42
43
44
45
46
47
48
49
50
51
52
53
54
55
56
57
58
59
60

model of ruptured abdominal aortic aneurysm. *Biomed Res Int* 2014;2014:857109.

18. Cheng P, Dai W, Wang F, Lu J, Shen M, Chen K, Li J, Zhang Y, Wang C, Yang J, Zhu R, Zhang H, Zheng Y, Guo C-Y, Xu L. Ethyl pyruvate inhibits proliferation and induces apoptosis of hepatocellular carcinoma via regulation of the HMGB1–RAGE and AKT pathways. *Biochem Biophys Res Commun* 2014;443(4):1162-1168.
19. Lee YM, Kim J, Jo K, Shin SD, Kim C-S, Sohn EJ, Kim SG, Kim JS. Ethyl Pyruvate Inhibits Retinal Pathogenic Neovascularization by Downregulating HMGB1 Expression. *J Diabetes Res* 2013;2013:8.
20. Ko H-K, Hsu W-H, Hsieh C-C, Lien T-C, Lee T-S, Kou YR. High expression of high-mobility group box 1 in the blood and lungs is associated with the development of chronic obstructive pulmonary disease in smokers. *Respirology* 2014;19(2):253-261.
21. Wang CM, Jiang M, Wang HJ. Effect of NF- κ B inhibitor on high-mobility group protein B1 expression in a COPD rat model. *Mol Med Rep* 2013;7(2):499-502.
22. Zhang Y, Li S, Wang G, Han D, Xie X, Wu Y, Xu J, Lu J, Li F, Li M. Changes of HMGB1 and sRAGE during the recovery of COPD exacerbation. *J Thorac Dis* 2014;6(6):734-741.
23. Lee DE, Trowbridge RM, Ayoub NT, Agrawal DK. High-mobility Group Box Protein-1, Matrix Metalloproteinases, and Vitamin D in Keloids and Hypertrophic Scars. *Plast Reconstr Surg Glob Open* 2015;3(6):e425.
24. Pandolfi F, Altamura S, Frosali S, Conti P. Key Role of DAMP in Inflammation, Cancer, and Tissue Repair. *Clin Ther* 2016;38(5):1017-1028.
25. Walker TG, Happer W. Spin-exchange optical pumping of noble-gas nuclei. *Reviews of Modern Physics* 1997;69(2):629-642.
26. Imai H, Fukutomi J, Kimura A, Fujiwara H. Effect of reduced pressure on the

1
2
3
4
5
6
7 polarization of ^{129}Xe in the production of hyperpolarized ^{129}Xe gas: Development
8
9 of a simple continuous flow mode hyperpolarizing system working at pressures as
10
11 low as 0.15 atm. Concepts in Magnetic Resonance Part B: Magnetic Resonance
12
13 Engineering 2008;33B(3):192-200.

14
15 27. Imai H, Kimura A, Hori Y, Iguchi S, Kitao T, Okubo E, Ito T, Matsuzaki T,
16
17 Fujiwara H. Hyperpolarized ^{129}Xe lung MRI in spontaneously breathing mice with
18
19 respiratory gated fast imaging and its application to pulmonary functional imaging.
20
21 NMR Biomed 2011;24:1343-1352.

22
23 28. Imai H, Matsumoto H, Miyakoshi E, Okumura S, Fujiwara H, Kimura A. Regional
24
25 fractional ventilation mapping in spontaneously breathing mice using
26
27 hyperpolarized ^{129}Xe MRI. NMR Biomed 2015;28:24-29.

28
29 29. Hamedani H, Clapp JT, Kadlecsek SJ, Emami K, Ishii M, Geftter WB, Xin Y, Cereda
30
31 M, Shaghaghi H, Siddiqui S, Rossman MD, Rizi RR. Regional Fractional
32
33 Ventilation by Using Multibreath Wash-in ^3He MR Imaging. Radiology
34
35 2016;279(3):917-924.

36
37 30. Ruppert K, Brookeman JR, Hagspiel KD, Mugler JP, III. Probing lung physiology
38
39 with xenon polarization transfer contrast (XTC). Magn Reson Med
40
41 2000;44(3):349-357.

42
43 31. Imai H, Kimura A, Iguchi S, Hori Y, Masuda S, Fujiwara H. Non-invasive
44
45 Detection of Pulmonary Tissue Destruction in a Mouse Model of Emphysema Using
46
47 Hyperpolarized ^{129}Xe MRS under Spontaneous Respiration. Magn Reson Med
48
49 2010;64(4):929-938.

50
51 32. Hardaker EL, Freeman MS, Dale N, Bahra P, Raza F, Banner KH, Poll C. Exposing
52
53 rodents to a combination of tobacco smoke and lipopolysaccharide results in an
54
55 exaggerated inflammatory response in the lung. Br J Pharmacol
56
57
58
59
60

1
2
3
4
5
6
7
8
9
10
11
12
13
14
15
16
17
18
19
20
21
22
23
24
25
26
27
28
29
30
31
32
33
34
35
36
37
38
39
40
41
42
43
44
45
46
47
48
49
50
51
52
53
54
55
56
57
58
59
60

2010;160(8):1985-1996.

33. Song HH, Shin IS, Woo SY, Lee SU, Sung MH, Ryu HW, Kim DY, Ahn KS, Lee HK, Lee D, Oh SR. Piscroside C, a novel iridoid glycoside isolated from *Pseudolysimachion rotundum* var. *subinegrum* suppresses airway inflammation induced by cigarette smoke. *J Ethnopharmacol* 2015;170:20-27.
34. Dregely I, Mugler JP, III, Ruset IC, Altes TA, Mata JF, Miller GW, Ketel J, Ketel S, Distelbrink J, Hersman FW, Ruppert K. Hyperpolarized Xenon-129 gas-exchange imaging of lung microstructure: first case studies in subjects with obstructive lung disease. *J Magn Reson Imag* 2011;33(5):1052-1062.
35. Kirby M, Svenningsen S, Owrangi A, Wheatley A, Farag A, Ouriadov A, Santyr GE, Etemad-Rezai R, Coxson HO, McCormack DG, Parraga G. Hyperpolarized ^3He and ^{129}Xe MR Imaging in Healthy Volunteers and Patients with Chronic Obstructive Pulmonary Disease. *Radiology* 2012;265(2):600-610.
36. Churg A, Cosio M, Wright JL. Mechanisms of cigarette smoke-induced COPD: insights from animal models. *Am J Physiol Lung Cell Mol Physiol* 2008;294(4):L612-631.
37. Beckett EL, Stevens RL, Jarnicki AG, et al. A new short-term mouse model of chronic obstructive pulmonary disease identifies a role for mast cell tryptase in pathogenesis. *J Allergy Clin Immunol* 2013;131(3):752-762.

1
2
3
4
5
6
7 Figure legends:
8
9
10

11 Figure 1. Example parametric maps of r_a derived from longitudinal studies of mice in
12 each of the three groups, from top to bottom: sham-instilled; CS and LPS model of
13 COPD; EP-treated. In all cases, the time course is shown horizontally.
14
15
16

17
18
19
20 Figure 2. Example parametric maps of f_D derived from longitudinal studies of mice in
21 each of the three groups, from top to bottom: sham-instilled; CS and LPS model of
22 COPD; EP-treated. In all cases, the time course is shown horizontally.
23
24
25
26

27
28
29
30 Figure 3. Box plots of the temporal change of mean r_a values for all mice, separated by
31 group. Significant differences between groups are indicated by solid lines, along with
32 the corresponding p values of significance (* $P < 0.05$; ** $P < 0.01$).
33
34
35
36

37
38
39
40 Figure 4. Box plots of the temporal change of mean f_D values for all mice, separated by
41 group. Significant differences between groups are indicated by solid lines, along with
42 the corresponding p values of significance (* $P < 0.05$; ** $P < 0.01$).
43
44
45
46

47
48
49
50 Figure 5. a) Box plots showing the mean MLI values obtained from mice in each of the
51 four groups, from left to right: sham-instilled; histological analysis (CS&LPS 4w), CS
52 and LPS model of COPD (CS&LPS10w); EP-treated. b) Representative examples of
53
54
55
56

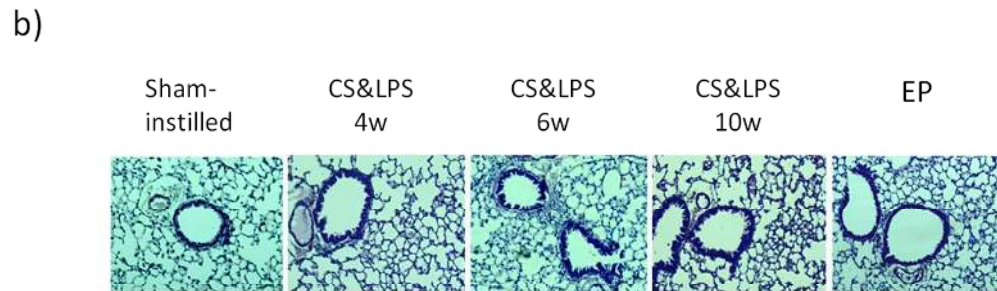
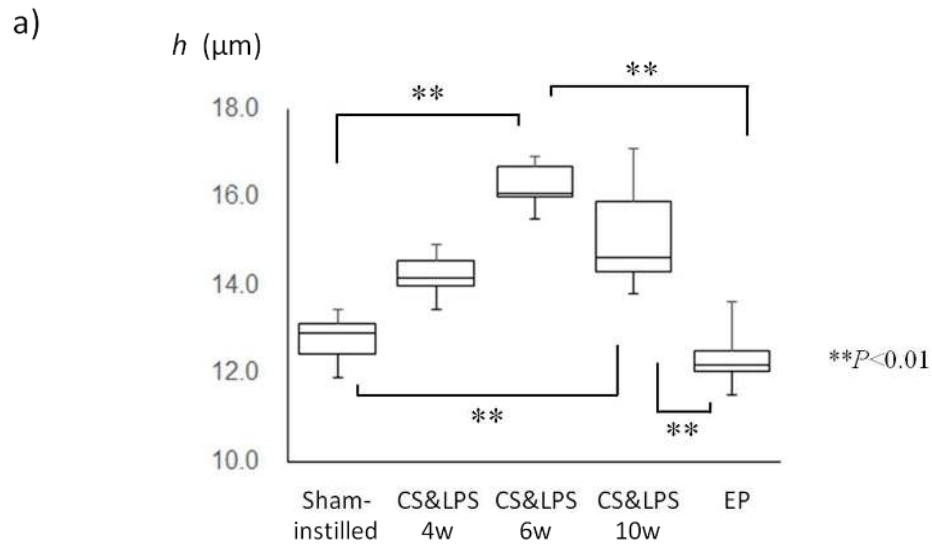
1
2
3
4
5
6
7
8
9
10
11
12
13
14
15
16
17
18
19
20
21
22
23
24
25
26
27
28
29
30
31
32
33
34
35
36
37
38
39
40
41
42
43
44
45
46
47
48
49
50
51
52
53
54
55
56
57
58
59
60

H&E stained histology slides obtained from 5 lung regions of one mouse chosen from each of the four groups. RU, right upper lobe; RM, right middle lobe; RL, right lower lobe; LU, upper region of the left lobe; LL, lower region of the left lobe. Note: mean values in a) represent the mean of the whole group; mean values in b) represent the mean for the selected mouse from each group.

Figure 6. a) Box plots showing the mean bronchial wall thickness (h) values obtained from mice in each of the four groups, from left to right: sham-instilled; histological analysis (CS&LPS 4w), CS and LPS model of COPD (CS&LPS10w); EP-treated after the 10 week experimental protocol. b) Representative examples of H&E stained histology slides obtained from the four groups.

Figure 7. Relationships between HPXe MRI-derived parameters of pulmonary function (r_a and f_D), and histology-derived parameters of lung structure (MLI and h) obtained from the sham-instilled (\square), EP-treated (\circ), and CS and LPS (\blacktriangle) mice after the 10 week experimental protocol. The Pearson's r value and P value of statistical significance are noted in each plot.

1
2
3
4
5
6
7 Supporting Figure S1. a) Box plots showing the mean bronchial wall thickness (h)
8 values obtained from mice in each of the five groups, from left to right:
9 sham-instilled; histological analysis (CS&LPS 4w and CS&LPS 6w), CS and LPS
10 model of COPD (CS&LPS10w); EP-treated after the 10 week experimental protocol. b)
11 Representative examples of H&E stained histology slides obtained from the five
12 groups.
13
14
15
16
17
18
19
20
21
22
23
24
25
26
27
28
29
30
31
32
33
34
35
36
37
38
39
40
41
42
43
44
45
46
47
48
49
50
51
52
53
54
55
56
57
58
59
60



Supporting Figure S1. a) Box plots showing the mean bronchial wall thickness (h) values obtained from mice in each of the five groups, from left to right: sham-instilled; histological analysis (CS&LPS 4w and CS&LPS 6w), CS and LPS model of COPD (CS&LPS10w); EP-treated after the 10 week experimental protocol. b) Representative examples of H&E stained histology slides obtained from the five groups.

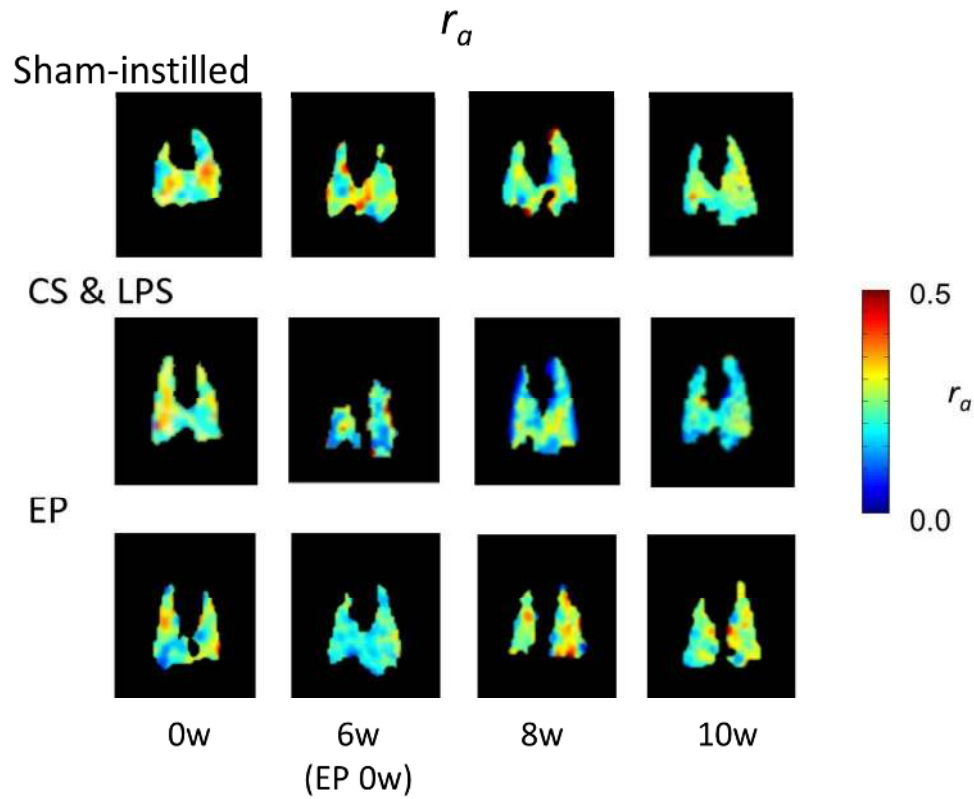


Figure 1. Example parametric maps of r_a derived from longitudinal studies of mice in each of the three groups, from top to bottom: sham-instilled; CS and LPS model of COPD; EP-treated. In all cases, the time course is shown horizontally.

118x118mm (300 x 300 DPI)

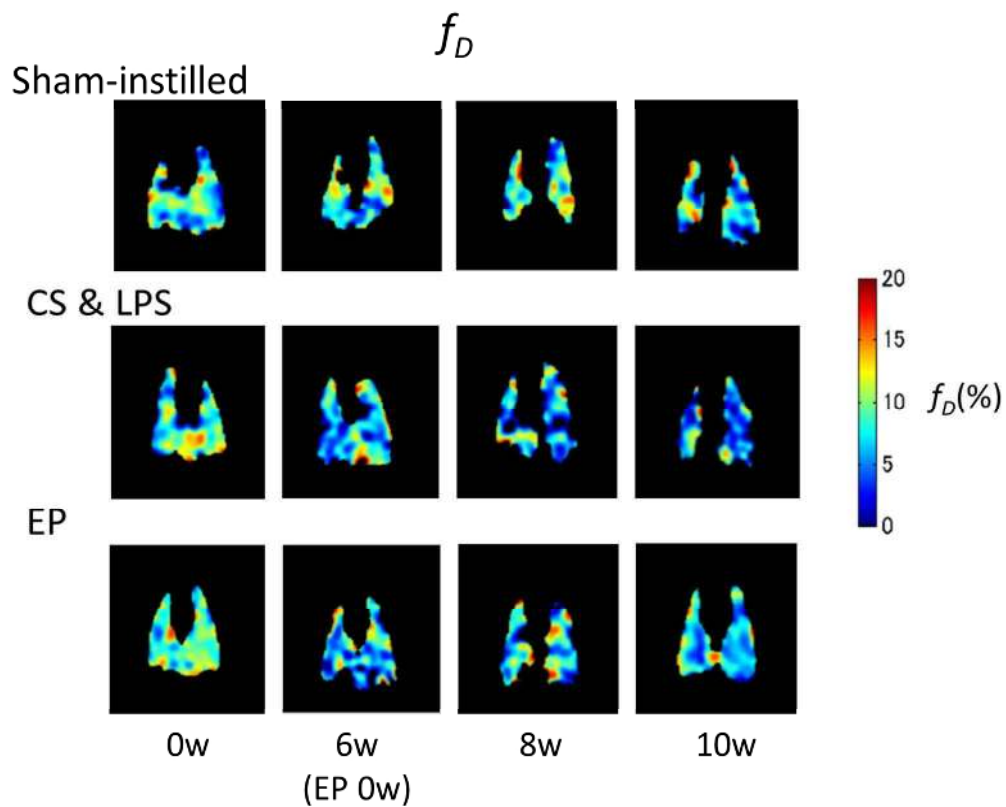


Figure 2. Example parametric maps of f_D derived from longitudinal studies of mice in each of the three groups, from top to bottom: sham-instilled; CS and LPS model of COPD; EP-treated. In all cases, the time course is shown horizontally.

118x118mm (300 x 300 DPI)

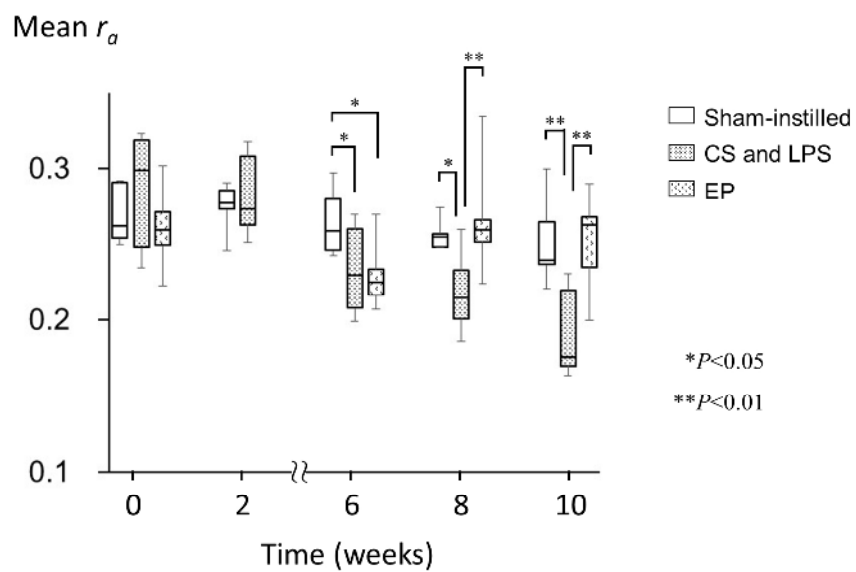


Figure 3. Box plots of the temporal change of mean r_a values for all mice, separated by group. Significant differences between groups are indicated by solid lines, along with the corresponding p values of significance (* $P < 0.05$; ** $P < 0.01$).

152x152mm (300 x 300 DPI)

1
2
3
4
5
6
7
8
9
10
11
12
13
14
15
16
17
18
19
20
21
22
23
24
25
26
27
28
29
30
31
32
33
34
35
36
37
38
39
40
41
42
43
44
45
46
47
48
49
50
51
52
53
54
55
56
57
58
59
60

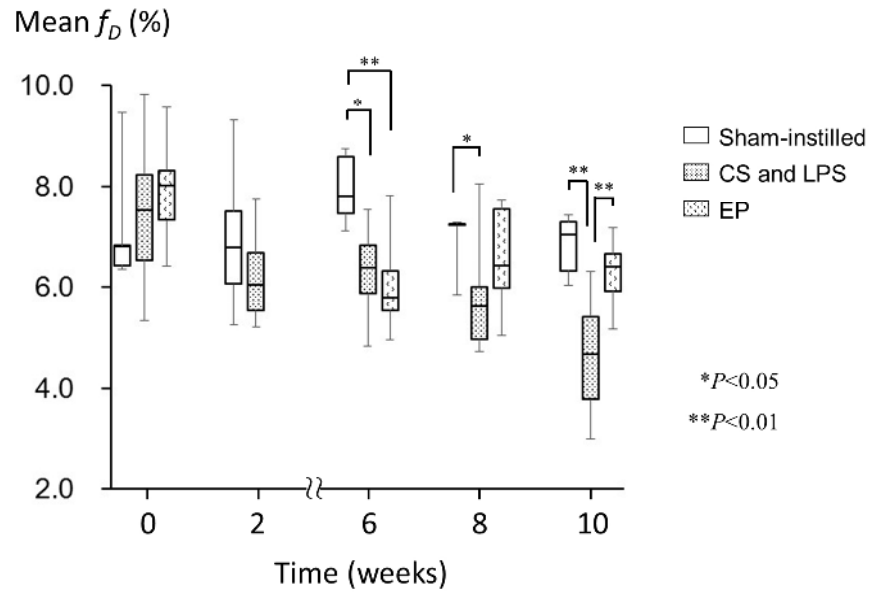


Figure 4. Box plots of the temporal change of mean f_D values for all mice, separated by group. Significant differences between groups are indicated by solid lines, along with the corresponding p values of significance (* $P < 0.05$; ** $P < 0.01$).

152x152mm (300 x 300 DPI)

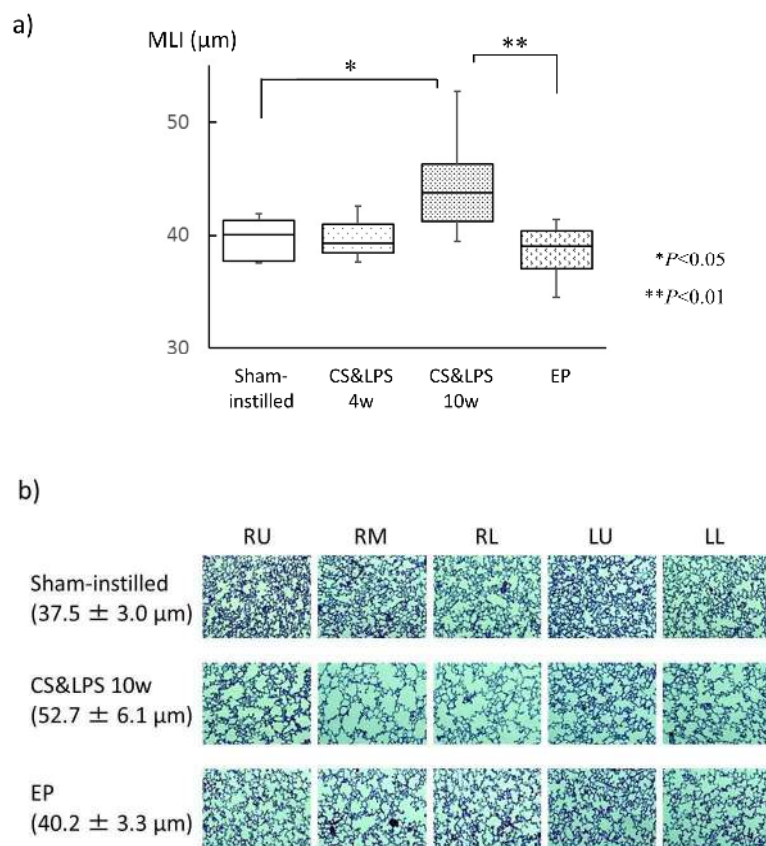


Figure 5. a) Box plots showing the mean MLI values obtained from mice in each of the four groups, from left to right: sham-instilled; histological analysis (CS&LPS 4w), CS and LPS model of COPD (CS&LPS10w); EP-treated. b) Representative examples of H&E stained histology slides obtained from 5 lung regions of one mouse chosen from each of the four groups. RU, right upper lobe; RM, right middle lobe; RL, right lower lobe; LU, upper region of the left lobe; LL, lower region of the left lobe. Note: mean values in a) represent the mean of the whole group; mean values in b) represent the mean for the selected mouse from each group.

203x203mm (300 x 300 DPI)

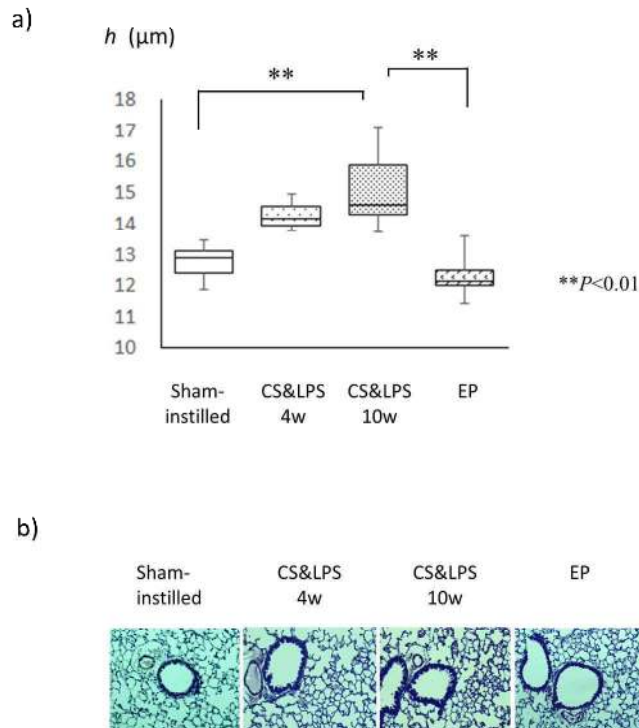


Figure 6. a) Box plots showing the mean bronchial wall thickness (h) values obtained from mice in each of the four groups, from left to right: sham-instilled; histological analysis (CS&LPS 4w), CS and LPS model of COPD (CS&LPS10w); EP-treated after the 10 week experimental protocol. b) Representative examples of H&E stained histology slides obtained from the four groups.

203x203mm (300 x 300 DPI)

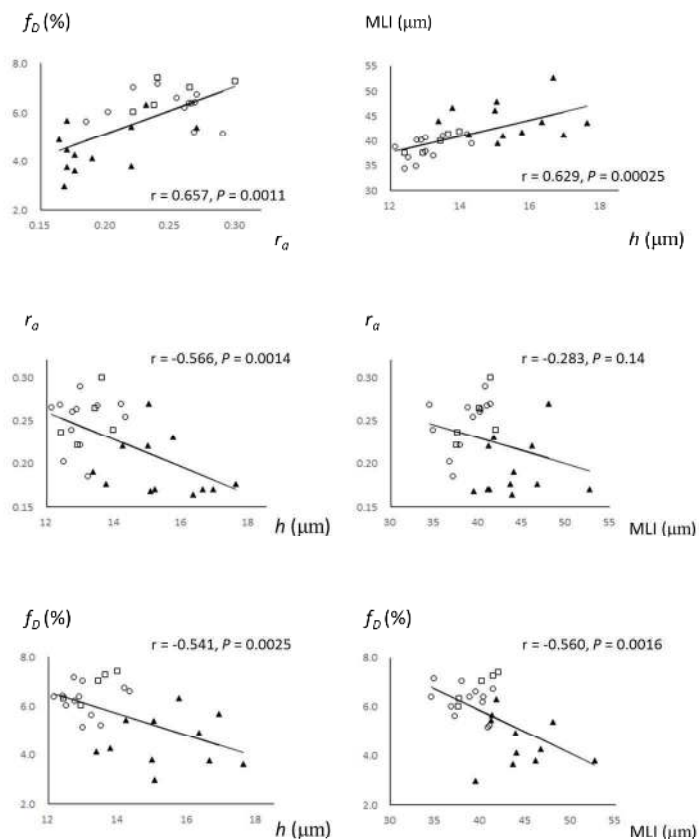


Figure 7. Relationships between HPXe MRI-derived parameters of pulmonary function (r_a and f_D), and histology-derived parameters of lung structure (MLI and h) obtained from the sham-instilled (□), EP-treated (○), and CS and LPS (▲) mice after the 10 week experimental protocol. The Pearson's r value and P value of statistical significance are noted in each plot.

152x152mm (300 x 300 DPI)